AD-A173 204 TRANSIENT LOSSES IN SUPERCONDUCTORS(U) NATIONAL BUREAU OF STANDARDS BOULDER CO ELECTROMAGNETIC TECHNOLOGY DIV R B GOLDFARB JUU 86 AFOSR-TR-86-0872 1/1

UNCLASSIFIED AFOSR-ISSA-82-00047 FFG 20/3 NL

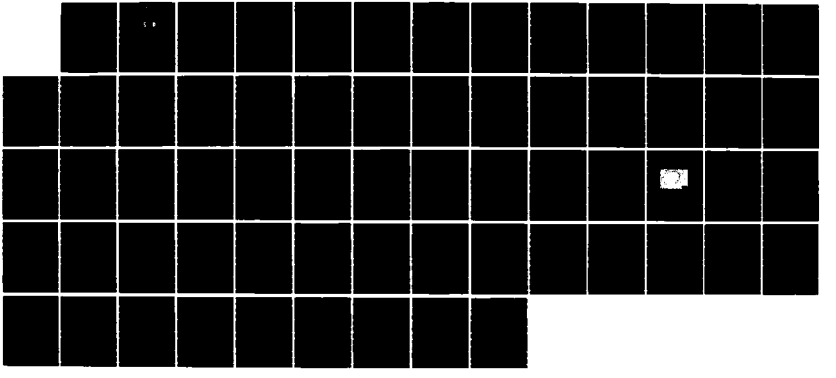

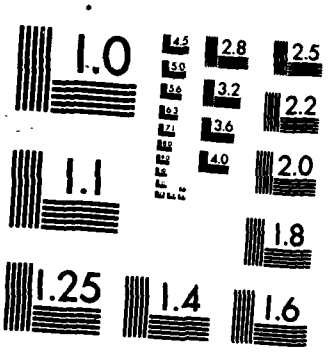

(2)

NBSIR 86-3053

AFOSR-TR- 86-0870

TRANSIENT LOSSES IN SUPERCONDUCTORS

Final Report

R. B. Goldfarb, Editor

National Bureau of Standards
U.S. Department of Commerce
Boulder, Colorado 80303

June 1986

UNCLASSIFIED
SECURITY CLASSIFICATION OF THIS PAGE

AD-A173 204

REPORT DOCUMENTATION PAGE

1a. REPORT SECURITY CLASSIFICATION: Unclassified	1b. RESTRICTIVE MARKINGS
2a. SECURITY CLASSIFICATION AUTHORITY	3. DISTRIBUTION / AVAILABILITY OF REPORT: Unlimited
2b. DECLASSIFICATION / DOWNGRADING SCHEDULE	
4. PERFORMING ORGANIZATION REPORT NUMBER(S): ~~NBSIR 86-3053~~	5. MONITORING ORGANIZATION REPORT NUMBER(S): AFOSR-TR-86-0872
6a. NAME OF PERFORMING ORGANIZATION: National Bureau of Standards; 6b. OFFICE SYMBOL (If applicable):	7a. NAME OF MONITORING ORGANIZATION: Air Force Office of Scientific Research
6c. ADDRESS (City, State, and ZIP Code): Boulder, Colorado 80303	7b. ADDRESS (City, State, and ZIP Code): Bolling Air Force Base, Washington, DC 20332
8a. NAME OF FUNDING / SPONSORING ORGANIZATION: AFOSR; 8b. OFFICE SYMBOL (If applicable): NE	9. PROCUREMENT INSTRUMENT IDENTIFICATION NUMBER: AFOSR-ISSA-82-00047, ~~85-00001~~, ~~84-00015~~, ~~85-00003~~
8c. ADDRESS (City, State, and ZIP Code): Same as 7b	10. SOURCE OF FUNDING NUMBERS: PROGRAM ELEMENT NO. 61102F; PROJECT NO. 2306; TASK NO. C1; WORK UNIT ACCESSION NO.

11. TITLE (Include Security Classification): TRANSIENT LOSSES IN SUPERCONDUCTORS (Unclassified)

12. PERSONAL AUTHOR(S): Goldfarb, R. B. (Editor)

13a. TYPE OF REPORT	13b. TIME COVERED	14. DATE OF REPORT (Year, Month, Day)	15. PAGE COUNT
Final Report	FROM 10/82 TO 9/85	1986 June	72

16. SUPPLEMENTARY NOTATION /

17. COSATI CODES			18. SUBJECT TERMS (Continue on reverse if necessary and identify by block number)
FIELD	GROUP	SUB-GROUP	
20	03		ac losses; hysteresis; magnetization; magnetometers; niobium-tin; niobium-titanium; superconductors; susceptibility; susceptometers; transient losses
20	12		

19. ABSTRACT

Under steady-state conditions, there are no losses in superconducting wires. However, when subjected to alternating or transient magnetic fields or transport currents, losses in type-II superconductors can become significant. This report deals with hysteresis losses at 4 K measured by magnetization and complex magnetic susceptibility. The theoretical and experimental relationships between ac susceptibility and magnetization as functions of dc field were examined in terms of the critical-state model, as developed by Carr and Clem. Minor-loop hysteresis loss was shown to be obtainable by direct measurement of loop area, from the imaginary component of ac susceptibility, and from the reversible susceptibility plus the critical current density or full-penetration field. Hysteresis and transport losses measured simultaneously in a Nb-Ti superconducting coil were found to agree substantially with the predictions of Minervini's two-dimensional model. Hysteresis loss measurements in a series of fine-filament Nb_3Sn superconductors showed that the effective filament diameter is a function of interfilament separation and local area ratio of matrix material to Nb. A review of internal fields in superconductors showed the importance of demagnetization factors and internal fields for the correct analysis of magnetic data. A theoretical method of calibrating ac susceptometers for cylindrical specimens, which is based on a mutual-inductance calculation, was developed.

20. DISTRIBUTION / AVAILABILITY OF ABSTRACT	21. ABSTRACT SECURITY CLASSIFICATION
☒ UNCLASSIFIED/UNLIMITED ☐ SAME AS RPT ☐ DTIC USERS	Unclassified

22a. NAME OF RESPONSIBLE INDIVIDUAL	22b. TELEPHONE (Include Area Code)	22c. OFFICE SYMBOL
Harold Weinstock	(202) 767-4933	AFOSR/NE

DD FORM 1473, 84 MAR — 83 APR edition may be used until exhausted. All other editions are obsolete.

SECURITY CLASSIFICATION OF THIS PAGE

UNCLASSIFIED

NBSIR 86-3053

TRANSIENT LOSSES IN SUPERCONDUCTORS

Final Report

R. B. Goldfarb, Editor

Electromagnetic Technology Division
Center for Electronics and Electrical Engineering
National Engineering Laboratory
National Bureau of Standards
Boulder, Colorado 80303

June 1986

Prepared for:
Air Force Office of Scientific Research
Bolling Air Force Base
Washington, DC 20332

U.S. DEPARTMENT OF COMMERCE, Malcolm Baldrige, Secretary

NATIONAL BUREAU OF STANDARDS, Ernest Ambler, Director

TRANSIENT LOSSES IN SUPERCONDUCTORS

Final Report

R. B. Goldfarb, Editor
Electromagnetic Technology Division
Center for Electronics and Electrical Engineering
National Engineering Laboratory
National Bureau of Standards
Boulder, Colorado 80303

Under steady-state conditions, there are no losses in superconducting wires. However, when subjected to alternating or transient magnetic fields or transport currents, losses in type-II superconductors can become significant. This report deals with hysteresis losses at 4 K measured by magnetization and complex magnetic susceptibility. The theoretical and experimental relationships between ac susceptibility and magnetization as functions of dc field were examined in terms of the critical-state model as developed by Carr and Clem. Minor-loop hysteresis loss was shown to be obtainable by direct measurement of loop area, from the imaginary component of ac susceptibility, and from the reversible susceptibility plus the critical current density or full-penetration field. Hysteresis and transport losses measured simultaneously in a Nb-Ti superconducting coil were found to agree substantially with the predictions of Minervini's two-dimensional model. Hysteresis loss measurements in a series of fine-filament Nb_3Sn superconductors showed that the effective filament diameter is a function of interfilament separation and local area ratio of matrix material to Nb. A review of internal fields in superconductors showed the importance of demagnetization factors and internal fields for the correct analysis of magnetic data. A theoretical method of calibrating ac susceptometers for cylindrical specimens, which is based on a mutual-inductance calculation, was developed.

Key words: ac losses; hysteresis; magnetization; magnetometers; niobium-tin; niobium-titanium; superconductors; susceptibility; susceptometers; transient losses.

TRANSIENT LOSSES IN SUPERCONDUCTORS

Final Report

EXECUTIVE SUMMARY

Under steady-state conditions, there are no losses in superconducting wires. However, when type-II superconductors are subjected to alternating or transient magnetic fields or transport currents, losses can become significant. Consequently, they are an important design consideration in many practical superconductor applications. AC losses may be categorized into hysteresis losses, eddy-current and coupling losses, and self-field losses.

This report deals mostly with hysteresis losses at 4 K. The experimental methods developed primarily involve the measurement of (1) magnetization as a function of field, and (2) complex magnetic susceptibility as functions of dc field and ac-field amplitude and frequency. Most measurements were made on variations of commercial multifilamentary Nb-Ti conductors with no transport current in longitudinal fields. However, some results are reported for Nb-Ti with transport current and Nb_3Sn conductors, both in transverse fields. In general, the experimental relationship between complex ac susceptibility and magnetization as a function of dc magnetic field was examined in terms of the critical-state model as developed by Carr and Clem. Good agreement between experiment and theory was found.

While the dc magnetic methods measure only the hysteresis component of total loss, hysteresis is usually the largest component of loss below 1 kHz. Additionally, magnetic hysteresis measurements give information on the remanent magnetization due to trapped flux in superconducting wires. This information is useful in selecting conductors for specific applications. For these reasons, it is likely that magnetic methods will emerge as a standard measurement technique for quantifying ac losses.

In addition to magnetic techniques, two other ways to measure transient losses in superconductors were evaluated. These methods were an electrical wattmeter and a calorimeter. These two other methods were found to be experimentally rather difficult compared to the magnetic methods. The electrical method requires the measurement of very small changes in phase angle between nonsinusoidal voltage and current. The calorimetric method requires the measurement of very small incremental helium flows above the normal static boil-off. More development would be required, compared to the magnetic methods, for the rapid acquisition of useful materials information.

Program Objectives

The following were program objectives and their related outputs:

1. Correlate hysteretic losses in a given material for different sample configurations.

Paper I: Hysteretic losses were studied in Nb-Ti superconductors with different filament diameters, numbers of filaments, and ratios of matrix

material to superconductor. Hysteresis decreased with decreasing filament diameter and was independent of conductor cross-sectional shape. The loss per volume of superconductor, expected to be independent of matrix-to-superconductor ratio, sometimes showed significant unexplained dependence.

2. Study the effect of matrix material on the losses for a given filamentary superconductor. Study coupling losses as a function of filament density and filament-matrix bonding.

Paper V: The effect of local area ratio of matrix material to superconductor was studied in fine-filament Nb_3Sn conductors. The hysteresis losses depended on the interfilament separation and area ratio.

3. Extend existing theoretical model for transient transport current and transient external field.

Paper IV: The two-dimensional model for shielding-hysteresis and transport-current losses was experimentally verified for the first time.

Results

A summary of significant results follows:

1. Hysteresis loss was shown to be accurately predicted within a few percent, using the London-Bean critical-state model, from the full-penetration field as a function of maximum applied field. It was shown that the full-penetration field could be deduced directly from the hysteresis loop, without reference to the critical current density. (See paper I.)

2. Minor-loop hysteresis loss was shown to be obtainable in three ways: by direct measurement of loop area, from the imaginary component of ac susceptibility, and from the reversible susceptibility plus the critical current density. The loss expressions derived by Carr were shown to be the same as those derived by Clem in the limit where the reversible susceptibility is zero. This was the first correlation of the different experimental magnetic methods. The relationships between complex magnetic susceptibility and permeability were discussed. (See paper II.)

3. A theoretical expression for the reversible susceptibility plus experimental measurements of full-penetration field were found to predict the measured real and imaginary components of ac susceptibility as functions of applied field using Clem's model. This was the first test of the applicability of the model to practical superconductors. The full-penetration field was found to be inversely proportional to applied longitudinal field, thus following a Kim-type relationship. The shape of the hysteresis loop was used to deduce the superconductor penetration depth and approximate the lower critical field. (See paper III.)

4. Hysteresis and transport losses measured simultaneously in a Nb-Ti superconducting coil were found to substantially agree with the predictions of Minervini's cylindrical model. This was the first experimental verification of the two-dimensional theory. (See paper IV.)

5. Systematic hysteresis loss measurements in a series of fine-filament Nb_3Sn superconductors showed that the effective filament diameter is a function of interfilament separation and local area ratio of matrix material to Nb. The effective filament diameter was obtained by applying the critical-state model to measured hysteresis loops. There would be little filament interaction due to bridging for Nb_3Sn interfilament separation greater than 2 μm. This was the first study of filament coupling in Nb_3Sn. The study is expected to have an impact on the design of practical wires. (See paper V.)

6. A review of internal fields in superconductors was prepared. The importance of demagnetization factors and internal fields for the correct analysis of magnetic data was discussed. The review will be a useful guide for the calibration of magnetometers used in measuring hysteresis losses in superconductors. (See paper VI.)

7. A new theoretical method of calibrating ac susceptometers for cylindrical specimens that is based on a mutual-inductance calculation was developed. The results were in excellent agreement with calibrations using standard reference materials. (See paper VII.)

8. A multifunction circuit was designed to protect instruments connected or coupled to a superconducting magnet against large voltage surges in the event of a quench. (See paper VIII.)

9. A review was prepared of the methods used for characterizing alloys, especially superconductors, with regard to matrix-to-superconductor volume ratio, filament radius, density, and weight and atomic percents. This review will be useful for some users and manufacturers of multifilamentary wires. (See paper IX.)

This project required the development of instrumentation for magnetic measurements and computer programs for data acquisition and processing. It resulted in the publication of five papers, the preparation of four other manuscripts (three of which will be submitted for publication), and participation in a workshop on problems in superconductivity [Cryogenics 24, 378 (1984)].

CONTENTS

Hysteretic losses in Nb-Ti superconductors

R. B. Goldfarb and A. F. Clark
Electromagnetic Technology Division, National Bureau of Standards, Boulder, Colorado 80303

When subjected to transient magnetic fields, superconductors exhibit losses. At low frequencies, most of the dissipation is hysteretic. Magnetization was measured in an axial field for eight multifilamentary Nb-Ti superconducting wires with different filament sizes and different ratios of copper to superconductor. The full-penetration field H_p was estimated from the high-field ends of the hysteresis loops. The estimate of H_p provides a method to assess the critical current density J_c. There was good agreement between measured losses and those predicted from H_p and the peak applied field.

INTRODUCTION

An ideal type I superconductor is perfectly diamagnetic below its critical temperature T_c and critical field H_c. This is a consequence of the Meissner effect,

$$B = \mu_0(H + M) = 0\,, \quad \chi = M/H = -1\,, \tag{1}$$

in SI units, where B is the magnetic flux density, H is the magnetic field strength, M is the magnetization, and χ is the susceptibility. The diamagnetism arises from circulating persistent surface currents.

In type II superconductors the pure Meissner state appears only below H_{c1}. Between H_{c1} and H_{c2} (lower and upper critical fields) the "mixed" state occurs in which surface currents coexist with magnetic vortices, usually containing one flux quantum each, formed by local persistent currents. These vortices are analogous to paramagnetic moments.[1] The effective magnetization (magnetic moment per unit volume), owing to surface and vortex currents, can be measured in the same way as the magnetization of magnetic materials.

According to the "critical state" model, as the applied field increases above H_{c1}, the magnetic flux and a current density J penetrate toward the center of the superconductor. The magnitude of J is J_c, the critical current density, taken to be independent of field. The field at which complete penetration occurs is termed the full-penetration field H_p. For a cylindrical filament with a field applied axially,

$$H_p = J_c r\,, \tag{2}$$

where r is the filament radius.

In "hard" type II superconductors, such as Nb-Ti, pinning sites impede the motion of flux vortices, which gives a higher value of J_c. Consequently, when the applied field is cycled, hysteresis occurs. Flux pinning is the largest source of bulk hysteresis, and hysteresis is the largest component of losses for ac fields below about 1 kHz. It is important to minimize these losses in non-dc superconducting-magnet applications in fusion, accelerators, and pulsed power sources. To minimize hysteresis, almost all commercial Nb-Ti wires are composed of many fine superconductor filaments, 1 to 25 μm in radius, within a thermally stabilizing Cu matrix. The weak diamagnetic contribution of the Cu to the effective magnetization is negligible.

Simple magnetic measurements can be useful to fabricators and users of superconductors. In this paper, measured hysteresis losses are compared to those predicted from theory for a number of superconductors.

EXPERIMENT

A vibrating-sample magnetometer (VSM) was used to obtain dc hysteresis loops at about 4.3 K. The magnetic field was supplied by a superconducting magnet. Field accuracy was estimated to be within $\pm$ 4 kA/m (50 Oe), and magnetization accuracy to be within $\pm$ 5%.

Each sample consisted of about 5–14 1.5-cm-long segments of insulated multifilamentary Nb-Ti wire, bundled together. For such lengths the filaments may be treated as uncoupled. The field and all measurements were along the longitudinal axis. There was no transport current applied to the wires.

Magnetization was calculated per volume of superconductor filaments. Demagnetization factor effects were negligible; the internal field was taken to be the same as the exter-

TABLE I. Physical properties of multifilamentary Nb-Ti superconductors.

Sample number	Dimensions without insulation (mm)	Number of filaments	Filament radius (μm)	Cu/Nb-Ti volume ratio
1	$d = 0.51$	180	12.2	1.46
2	0.57×0.84	132	13.0	4.98
3	$d = 0.68$	2046	4.3	2.08
4	$d = 0.64$	180	15.0	1.50
5	0.52×0.70	180	16.4	1.30
6	0.64×0.89	168	19.9	1.59
7	$d = 1.01$	114	19.5	4.84
8	0.63×0.88	240	19.3	0.91

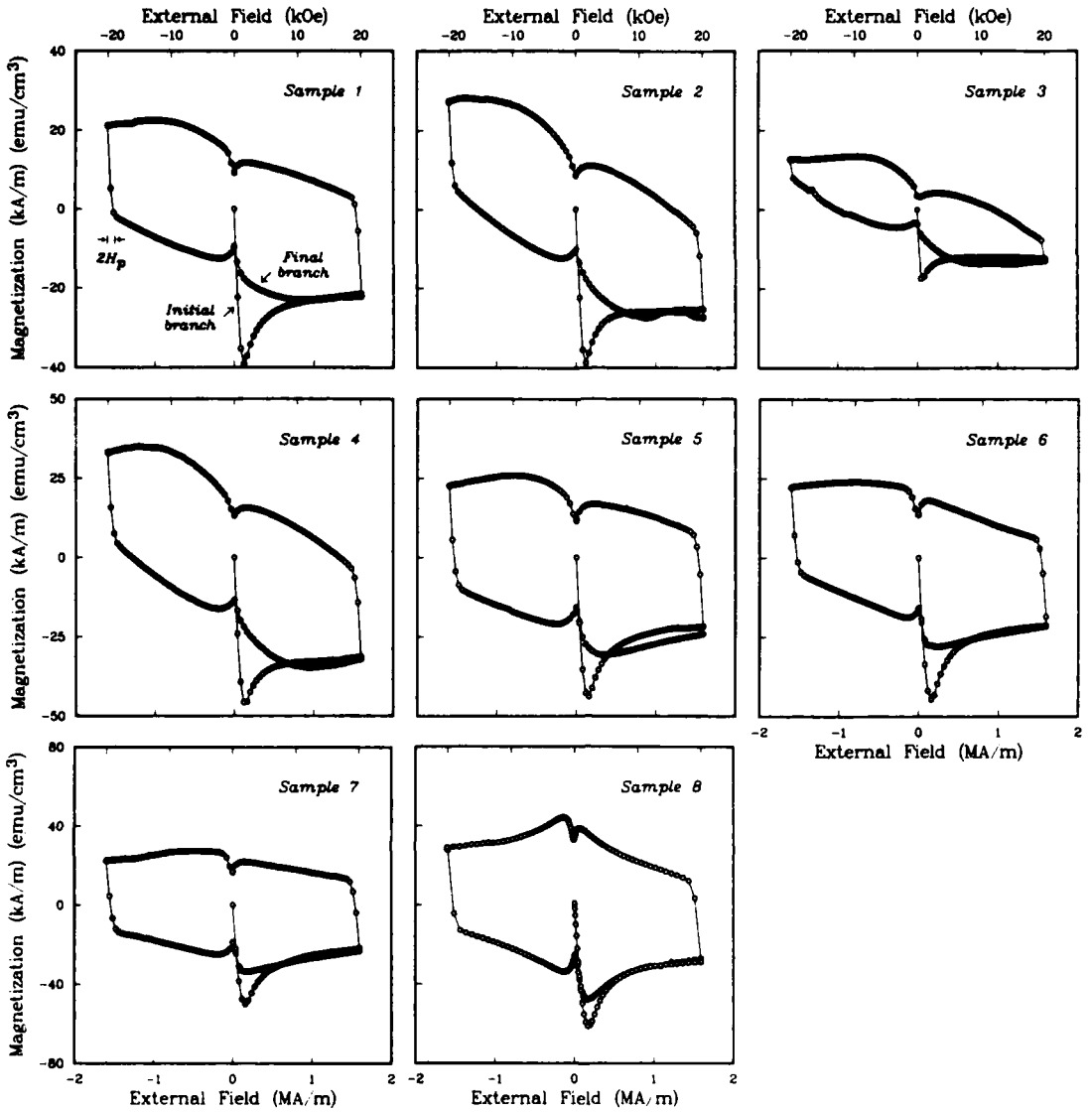

FIG. 1. dc hysteresis loops for eight multifilamentary Nb-Ti superconductors. Note that the vertical scales are not all the same.

nal applied field. Before each set of measurements was made, the sample was warmed above T_c (about 10.2 K for Nb-Ti) and then cooled in zero field.

MEASUREMENT OF HYSTERESIS

Table I summarizes the physical properties of the superconductor wires studied. Figure 1 shows the hysteresis loops for the samples for a peak applied field H_0 of 1.6 MA/m (20 kOe). Occasional spurious nonsmooth behavior is accounted for by slight deviations in temperature during measurement. The area enclosed by each loop is equal to the loss W,

$$W = \mu_0 \oint H\, dM \cong \mu_0 \oint M\, dH\,, \tag{3}$$

where H ranges from $+H_0$ to $-H_0$.

The full-penetration field H_p can be estimated from the hysteresis loop. As the loop is traversed, the filaments go from full penetration in one direction to full penetration in the other direction. Therefore, at a high-field end of the loop, H_p is approximately one-half the field required to reverse the magnetization. This reversal field $2H_p$ is determined by a peak in d^2M/dH^2 and is indicated on the loop for sample 1 in Fig. 1.

For the case when the peak applied field H_0 is greater than H_p, Carr derived an expression for the loss, assuming J_c to be independent of magnetic field.[2] In SI units,

$$W = (4\mu_0 H_0 H_p/3)(1 - H_p/2H_0)\,. \tag{4}$$

Clearly H_0 is much larger than H_p for the loops in Fig. 1.

TABLE II. Hysteresis loss W for a peak field H_0 of 1.6 MA/m (20 kOe).

Sample number	Loss from loop area (kJ/m³)	H_p (kA/m)	H_p (Oe)	Loss from H_p (kJ/m³)
1	114	45	550	120
2	116	45	550	120
3	50	20	250	50
4	152	50	650	130
5	158	65	800	170
6	141	60	750	160
7	177	65	800	170
8	224	80	1000	210

Losses calculated numerically using Eq. (3) and computed using Eq. (4) are compared in Table II. Considering the approximate nature of the H_p determination, the agreement is good.

Based on Eq. (2), J_c can be estimated from H_p. This could be useful for new superconductor materials where it is difficult to measure J_c directly in wire samples. In this paper, J_c is the critical current density for the filaments, not the entire wire. For $H_0 \gg H_p$, Eqs. (4) and (2) give J_c in terms of measured loop area W:

$$J_c = 3W/4\mu_0 H_0 r. \tag{5}$$

COMPARISON OF HYSTERESIS LOOPS

Although different wires from different manufacturers are listed in the tables, some comparisons may be made. Equations (4) and (2) indicate the well-known fact that hysteresis decreases with decreasing filament radius. This is illustrated in a comparison of the losses in samples 1 and 4. The wires are virtually identical except for filament radius. An extreme case is sample 3, with a large number of very fine filaments. A comparison of samples 4 and 5 shows that conductor geometry (round vs. rectangular cross section) has no significant effect on the loss.

Since magnetization is plotted per unit volume of superconductor (Nb-Ti) rather than per unit wire volume, the copper-to-superconductor volume ratio is not expected to have a large effect on the magnetization values. A comparison of samples 1 and 2 shows little difference. However, samples 6 and 8, with similar filament radii, show significant differences in measured losses.

The shapes of the loops are somewhat intriguing. The loops for samples 1, 2, 3, and 4 are generally trapezoidal and negatively sloped. Those for samples 5, 6, 7, and 8 are generally hexagonal and more hysteretic. The difference in types is highlighted if the initial branch of each loop is compared to the final branch (see Fig. 1, sample 1). For the hexagonal set, there is an attempt, upon increasing the field from zero, to retrace the peak of the initial branch. These curves most resemble the ideal reversible magnetization curve that is expected from the critical state model.

CONCLUSION

Measured hysteresis losses for eight multifilamentary Nb-Ti superconductors were found to be in good agreement with predicted values based on the maximum applied field H_0 and the full-penetration field H_p. The latter, a function of critical current density J_c and filament radius r, was estimated from the hysteresis loop. This estimate of H_p can be a convenient method of assessing the critical current density.

ACKNOWLEDGMENT

This work was sponsored by the Air Force Office of Scientific Research.

[1] W. J. Carr, Jr., IEEE Trans. Magn. MAG-21, 355 (1985).
[2] W. J. Carr, Jr., *AC Loss and Macroscopic Theory of Superconductors* (Gordon and Breach, New York, 1983), p. 70.

MAGNETIC HYSTERESIS AND COMPLEX SUSCEPTIBILITY AS MEASURES OF AC LOSSES IN A MULTIFILAMENTARY NbTi SUPERCONDUCTOR

R. B. Goldfarb and A. F. Clark
Electromagnetic Technology Division
National Bureau of Standards
Boulder, Colorado 80303

Abstract

Magnetization and ac susceptibility of a standard NbTi superconductor were measured as a function of longitudinal dc magnetic field. The ac-field-amplitude and frequency dependences of the complex susceptibility are examined. The magnetization is related to the susceptibility by means of a theoretical derivation based on the field dependence of the critical current density. Hysteresis losses, obtained directly from dc hysteresis loops and derived theoretically from ac susceptibility and critical current density, were in reasonable agreement.

Introduction

When subjected to alternating or transient magnetic fields, superconducting wires exhibit losses. These may be categorized into hysteresis losses, eddy-current losses, coupling losses, and self-field losses. Bulk hysteresis losses are frequency independent and arise mostly from flux pinning in the superconducting filaments. There may be, in addition, hysteretic losses due to pinning at the filament surface. At high frequencies, eddy-current losses occur within the matrix and on the wire surface (skin effect). Coupling losses in the matrix, important over about 1 kHz, are caused by the transfer of coupling currents between filaments. If there is a transport current, matrix eddy-current losses arise from the self field.

There are a few general methods of measuring ac losses in superconductors. The most direct is calorimetric, in which a superconducting coil is exposed to transient fields and the dissipated heat is measured by the boil-off of liquid helium. Another method is electrical, by measuring the phase angle between voltage and current. Wattmeters work on this principle.

The final methods are magnetic. Magnetization measurements are possible because magnetic moments are associated with circulating persistent surface currents and, in type-II superconductors in the mixed state, flux vortices. There are basically two types of magnetic methods. In the first, magnetization (magnetic moment per unit volume) is measured directly using, for example, a vibrating-sample magnetometer. Though lock-in detection at the frequency of vibration is used, this is a dc measurement, since the time required to cycle the field is on the order of 30 minutes. Measurements may be made while slowly ramping or stepping the field. The latter gives more accurate results if there is any imbalance in the pick-up coils.

In the second type of magnetic measurement, a sinusoidal ac field is applied (sometimes superimposed upon a dc field) and the derivative of the magnetization is detected by induction in a pickup coil. If the pickup coil is uncompensated, the induced voltage is proportional to the permeability μ. If the coil is compensated (i.e., zero voltage when no sample is present), the induced voltage is proportional to the susceptibility χ. In SI units,

$$\mu = \mu' - i\mu'' = \mu_0(1+\chi) = \mu_0(1+\chi' - i\chi''), \quad (1a)$$

$$\mu' = \mu_0(1+\chi'), \quad (1b)$$

$$\mu'' = \mu_0\chi'', \quad (1c)$$

where single primes indicate the real (dispersive, inductive) components, the double primes indicate the imaginary (absorptive, resistive, loss) components, and μ_0 is the permeability of free space. The induced voltages may be integrated with respect to field (or with respect to time, since field is swept as a function of time) to yield the frequency-dependent magnetization.[1]

The area enclosed by the dc or low-frequency ac hysteresis loop of magnetization vs. field is a direct measure of the hysteresis loss. Alternately, the imaginary component of susceptibility (or permeability) at low frequencies is an indirect measure of the hysteresis loss. This paper will discuss dc hysteresis loops and complex susceptibility. The commonly used method of integrated voltages will not be discussed. The conductor carries no transport current.

Experimental Methods

DC hysteresis loops at about 4.1 K were obtained using a vibrating-sample magnetometer (VSM). Field values up to 1.6 MA/m (20 kOe) were determined from the current in a multifilamentary Nb-Ti superconducting magnet. No correction was made for trapped flux; zero-field-value errors are thus estimated to be ±4 kA/m (50 Oe).

AC susceptibility was measured at 4 K with a lock-in amplifier and a compensated susceptometer of the type described in Ref. 2. If the induced waveform is nonsinusoidal, the lock-in amplifier will detect only the fundamental-frequency component. Losses that appear as harmonics are not detected. Therefore, this method is most suitable for relatively small ac field amplitudes. For very small ac field amplitudes, χ'' is known to be about zero, and this fact is used to adjust the phase ϕ on the lock-in amplifier:

$$\chi' = |\chi|\cos\phi, \quad (2a)$$

$$\chi'' = |\chi|\sin\phi. \quad (2b)$$

The phase setting was kept constant for all fields, but was readjusted for each frequency. The background signal in the absence of a sample was subtracted from all measurements. The susceptometer was positioned in the bore of the same superconducting magnet as used with the VSM. Both apparatus were computer controlled. Magnetization and susceptibility accuracies are estimated to be within 5%.

The sample consisted of an insulated, Nb-Ti wire, cut into 14 straight segments 1.5 cm long, and bundled together. At low frequencies and for short samples (or short twist pitch), the filaments may be taken to be uncoupled. The field and all measurements were along the longitudinal axis. Before each set of measurements was made, the sample was warmed to above its critical temperature and then cooled in zero field. Demagnetization-factor corrections were negligible; the internal field was taken to be the same as the external applied

Manuscript received September 10, 1984.

0018-9464/85/0300-0332$01.00 © 1985 IEEE

field. Magnetization and susceptibility were calculated per volume of superconductor filaments. Mass and volume measurements were made on a length of the wire, before and after dissolving the Cu matrix in HNO_3, to experimentally determine the filament radius and the volume and density of NbTi. The characteristics of the wire are given in Table I.[3]

Table I. Characteristics of NBS SRM 1457

Number of filaments:	180
Filament radius:	12.20 μm
Copper-to-NbTi volume ratio:	1.456
Density of NbTi alloy:	6.004 g/cm³
NbTi-to-insulated-wire mass ratio:	0.3025

AC Field Dependence of Complex Susceptibility

The ac susceptibility of the sample was measured for a few field amplitudes and frequencies as the dc bias field was stepped. Figures 1a-e show a comparison of the results. Only three branches are shown for each case to avoid redundancy. The shapes of the χ' and χ'' curves are dependent upon both field amplitude and frequency. The frequency dependence is small, which is evidence that hysteresis is the major loss mechanism. For the smaller field amplitudes there are large differences between ascending and descending branches, and the branches are not symmetrical for positive and negative external dc fields (Figs. 1a-c). These effects may be attributed to relatively large filament-surface losses when the ac field is small. Bussière and Clem[4] discuss the applicable case when losses are associated with the bending of vortices trapped at a high angle to the surface, and the field is much less than the lower critical field H_{c1}. Short samples facilitate this effect.

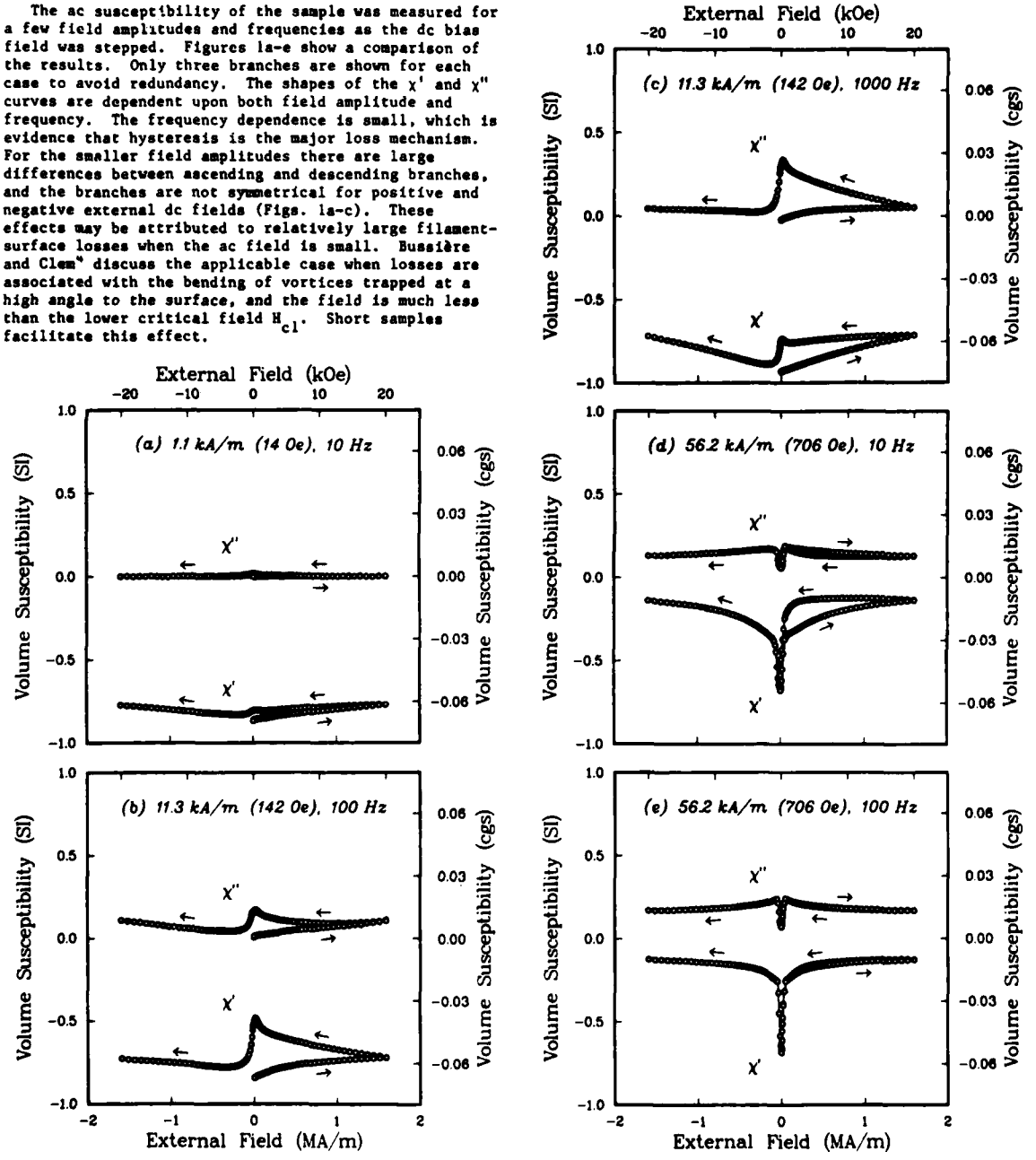

Figure 1. Imaginary (χ'') and real (χ') components of ac susceptibility as a function of applied longitudinal dc field at 4 K. AC field amplitudes and frequencies are shown.

Erratum: Page 333, first column, next-to-last sentence: "field" should be "ac field"

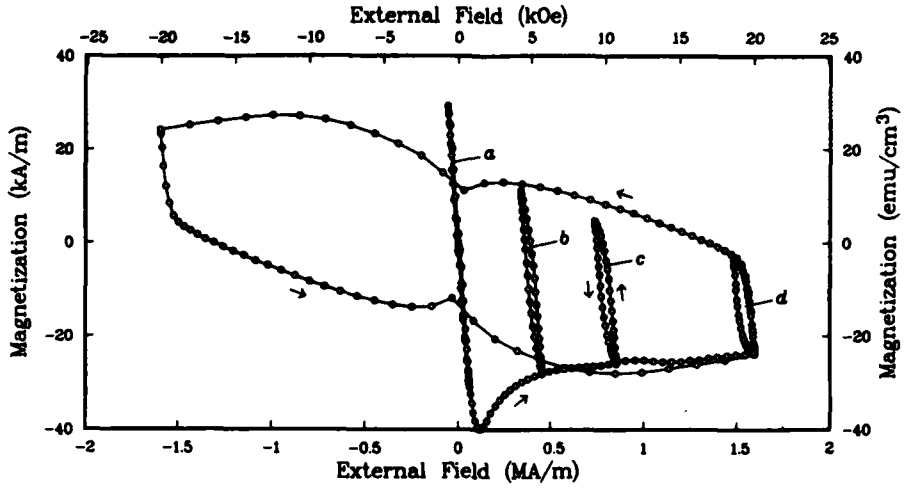

Figure 2. Magnetization M vs. dc field H at 4.1 K obtained with a VSM. The initial branch for zero trapped flux and four minor loops (a-d) are shown.

Theoretical Derivation of Complex Susceptibility

The following theoretical description of complex susceptibility is based on the development by Clem for the case of bulk-pinning hysteretic losses in type-II superconductors.[5] The model applies when the ac field amplitude is small and the field equations can be linearized. It will be shown that the dc hysteresis loop and the field dependence of the critical current density are predictive of the ac susceptibility.

The critical current as a function of transverse field[6] for the sample was converted to critical current density J_c using the total superconductor cross-sectional area (not including matrix material). A good fit was obtained to the Kim equation,

$$J_c(H) = J_c(0)/(1+H/H_0), \qquad (3)$$

for fields H up to 4.8 MA/m (60 kOe). The adjustable parameters $J_c(0)$ and H_0 were found to be 9.2 GA/m² and 1.1 MA/m (14 kOe), respectively. While the longitudinal-field J_c is larger than the transverse-field J_c, they are, of course, identical at zero field. The full-penetration longitudinal field H_p is a function of H owing to the field dependence of J_c:

$$H_p(H) = J_c r, \qquad (4)$$

where r is the filament radius. It is useful to define a parameter x as

$$x(H) = h/H_p = h/J_c r, \qquad (5)$$

where h is the peak amplitude of the ac field that is superimposed upon H.

As shown by Clem and using Eqs. 1, the complex susceptibility may be expressed in terms of an idealized differential susceptibility for type-II superconductors χ_{rev}:

$$\chi' = (1+\chi_{rev})g_1(x)-1, \qquad (6)$$

$$\chi'' = (1+\chi_{rev})g_2(x), \qquad (7)$$

where

$$\chi_{rev} = dM_{rev}/dH \qquad (8)$$

where M_{rev} is the reversible magnetization, and

$$g_1(x) = x-5x^2/16, \qquad 0 < x < 1, \qquad (9a)$$

$$g_1(x) = [(-1+x-5x^2/16)\theta + (-4/3x+2-7x/4+13x^2/24)\sin\theta + (-1/2+x/2-x^2/6)\sin2\theta + (-x/12+x^2/24)\sin3\theta + (-x^2/192)\sin4\theta]/\pi + 1, \qquad x > 1, \qquad (9b)$$

where $\theta(x) = 2\sin^{-1}(x^{-1/2})$, $\theta(1) = \pi$, $\theta(\infty) = 0$, and

$$g_2(x) = (4x-2x^2)/3\pi, \qquad 0 < x < 1, \qquad (10a)$$

$$g_2(x) = (4/x-2/x^2)/3\pi, \qquad x > 1. \qquad (10b)$$

Using Eqs. 6 and 7, χ' and χ'' will be calculated for the sample. The major hysteresis loop for the sample is shown in Fig. 2. The lower critical field H_{c1} is

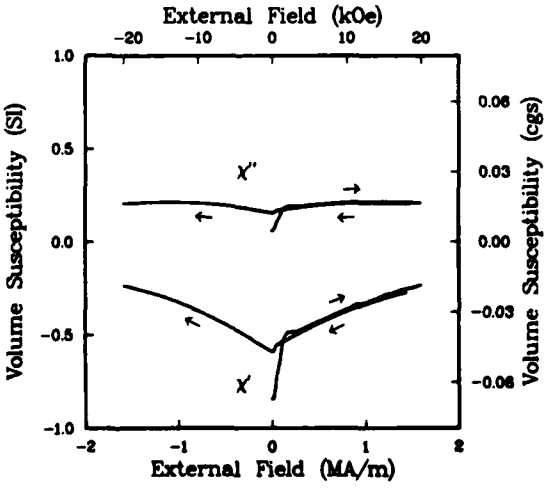

Figure 3. Imaginary (χ'') and real (χ') components of ac susceptibility calculated for an ac field amplitude of 56.2 kA/m (706 Oe) using the theoretical model, the data in Fig. 2, and the field dependence of J_c (Eq. 3).

Table II. Comparison of hysteretic losses obtained by dc and ac methods for a field amplitude of 56.2 kA/m (706 Oe).

Center field (kA/m)	(kOe)	Loss from minor-loop area (kJ/m^3)	Loss from χ'' Eq. 11 (kJ/m^3)	Loss from Eqs. 12, 13 (kJ/m^3)
0	0	0.6	0.7	0.9
400	5.0	1.3	2.0	2.1
800	10.0	1.4	1.8	2.6
1540	19.3	1.3	1.6	2.6

about 0.12 MA/m (1.5 kOe). The tangent to the curve at any H is the differential susceptibility χ_{dc}. As an approximation, χ_{dc} will be used for χ_{rev}. This is somewhat reasonable for the initial branch of the hysteresis loop, but rather unreasonable for the later irreversible branches. However, theoretical χ_{rev} and experimental χ_{dc} are both about zero for fields much larger than H_{c1} and therefore do not greatly affect the computation.

A program was written to compute, for each value of H and χ_{dc}, the predicted $J_c(H)$, $H_c(H)$, $x(H)$, $g_1(x)$, $g_2(x)$, $\chi'(x)$, and $\chi''(x)$, given r and h. For $h = 56.2$ kA/m (706 Oe), χ' and χ'' as computed are plotted as a function of H in Fig. 3. As in Fig. 1, only the first three branches are shown. No adjustable parameters were used. A comparison with actual measured χ' and χ'' in Figs. 1d,e shows good agreement in both shape and magnitude. Ideally, the computed curves in Fig. 3 would be symmetrical with respect to the external dc field and show no difference between the initial segment and the return portion, as expected from critical state theory.[5] Deviations from this are because χ_{dc} was used instead of χ_{rev}.

Hysteresis Loss

In this section, the minor loops in Fig. 2 are examined. The loss corresponding to each is calculated in three ways: minor-loop area, from χ'', and from J_c.

The energy loss per unit volume per cycle is[5]

$$W = \pi\mu_0 h^2 \chi''. \tag{11}$$

Substituting for χ'' using Eqs. 7, 10b, and 5 for full field penetration ($x > 1$),

$$W = (1+\chi_{rev})(4\mu_0 h J_c r/3)(1-J_c r/2h). \tag{12}$$

Except for the factor $(1+\chi_{rev})$, the same equation is derived, in cgs emu, by Carr.[7] But for $H \gg H_{c1}$, $\chi_{rev} \approx 0$. For partial field penetration ($x < 1$), using Eqs. 7, 10a, and 5, Eq. 11 may be expressed as

$$W = (1+\chi_{rev})(4\mu_0 h^3/3J_c r)(1-h/2J_c r), \tag{13}$$

again similar to Carr's expression for this case.

Figure 2 shows four minor dc hysteresis loops for the sample determined experimentally with the VSM. The peak amplitude for each minor loop is 56.2 kA/m (706 Oe). The area enclosed by each loop was calculated numerically by

$$W = \mu_0 \oint H\, dM = \mu_0 \oint M\, dH. \tag{14}$$

This hysteresis loss is compared in Table II to the losses derived from Eq. 11, using χ'' measured at 10 Hz in 56.2 kA/m (706 Oe) peak field (Fig. 1d). Another comparison can be made with losses obtained using Eqs. 12 and 13, with J_c (at the center field) from Eq. 3. For the first minor loop, $x < 1$. Once again, χ_{rev} is approximated by χ_{dc} from the initial branch of the hysteresis loop. The agreement is reasonable, indicating that hysteretic losses may be measured directly with a hysteresis loop, or estimated by measurement of the imaginary component of low-frequency ac susceptibility, or from a reasonable estimate of $J_c(H)$.

Possible inaccuracies owing to the following should be considered: (1) $J_c(H)$ was measured in transverse rather than longitudinal field; (2) losses are not entirely hysteretic; (3) induced voltage in susceptometer pickup coil contains higher-order harmonics; (4) applied ac field amplitude was not small enough to allow linearized field equations. Only the first of these is believed to be of significance, affecting the data in the last column of Table II.

Conclusion

The technique used to measure hysteretic losses might depend on one's application. If a field is stepped slowly, a dc hysteresis loop is obtained. If an alternating field is swept and the induced voltage integrated, an ac hysteresis loop may be obtained. For the general case, a dc bias field may be superimposed upon the stepped or alternating field. If the induced voltage is not integrated, but separated into real and imaginary parts, the complex susceptibility is obtained. Often, an ac susceptibility measurement is a convenient method. In this paper, it was shown that the complex susceptibility in an ac field could be reasonably predicted from the dc hysteresis loop, the critical current density, and the filament radius. Hysteresis losses obtained directly (Eq. 14) were compared to those obtained indirectly using experimental measurements of χ'' (Eq. 11) and average values of J_c and χ_{dc} (Eqs. 12 and 13).

Acknowledgments

The authors are grateful to J. R. Clem for critical comments on an earlier draft of the manuscript. This work was sponsored by the Air Force Office of Scientific Research.

References and Footnotes

1. W. A. Fietz, "Electronic Integration Technique for Measuring Magnetization of Hysteretic Superconducting Materials," Rev. Sci. Instrum. 36, pp. 1621-26 (1965).
2. R. B. Goldfarb and J. V. Minervini, "Calibration of AC Susceptometer for Cylindrical Specimens," Rev. Sci. Instrum. 55, pp. 761-64 (1984).
3. NbTi wire, Standard Reference Material 1457 for critical current measurements, available from Office of Standard Reference Materials, National Bureau of Standards, Gaithersburg, MD 20599. The data on this wire in Table I are not certified by NBS.
4. J. F. Bussière and J. R. Clem, "Effect of trapped magnetic flux on ac losses of Nb_3Sn," IEEE Trans. Magn. MAG-15, pp. 264-67 (1979).
5. J. R. Clem, "AC Losses in Type-II Superconductors," Ames Lab. Tech. Rept. IS-M 280, 1979.
6. Critical current was measured at 4 K by L. F. Goodrich using a transport current technique with a 0.2 μV/cm criterion. The self-field contribution was not included. The demagnetization field, which would correct values of applied field, is about 0.6% at 1.6 MA/m (20 kOe) and 0.2% at 4.8 MA/m (60 kOe).
7. W. J. Carr, Jr., AC Loss and Macroscopic Theory of Superconductors, New York: Gordon and Breach, 1983, p. 70.

International Cryogenic Materials Conference - ICMC
Cambridge, Massachusetts - August 1985
Paper DZ-8
To be published in:
"Advances in Cryogenic Engineering (Materials)"
Vol. 32, R. P. Reed and A. F. Clark, eds.
Plenum Press, New York (1986)

AC LOSSES IN Nb-Ti MEASURED BY MAGNETIZATION AND COMPLEX SUSCEPTIBILITY

R. B. Goldfarb and A. F. Clark
Electromagnetic Technology Division
National Bureau of Standards
Boulder, Colorado

ABSTRACT

DC magnetization and complex ac susceptibility were measured at 4 K as functions of longitudinal dc field for a multifilamentary Nb-Ti superconductor with no transport current. Minor hysteresis loops were obtained in the dc measurements. The full-penetration field, H_p, a function of applied field, H, was deduced directly for each minor loop. The values for H_p were fit to the Kim-type equation, $H_p(H) = H_p(0)/(1+H/H_k)$, where $H_p(0)$ and H_k are constants. The minor hysteresis-loop areas gave losses that were in excellent agreement with Carr's theoretical critical-state equation, $W = (4\mu_0 H_0 H_p/3)(1-H_p/2H_0)$, where H_0 is the maximum applied field for each loop.

An expression was obtained for the ideal reversible differential susceptibility: $\chi_{rev} = \phi_0/8\pi\mu_0(H-H_{c1})\lambda^2$, where ϕ_0 is the flux quantum, H_{c1} is the lower critical field, and λ is the penetration depth. H_{c1} and λ for the sample were deduced from the shape of the major hysteresis loop. Clem's theoretical expressions for the real (χ') and imaginary (χ'') components of ac susceptibility are functions of χ_{rev}, H_p, and ac field amplitude, h. The predicted susceptibilities based on these expressions were in good agreement with measured curves of χ' and χ'' as functions of h and H. The measured χ' and χ'' were independent of frequency up to 1 kHz, as expected when bulk hysteresis is the primary loss mechanism.

INTRODUCTION

In an earlier work[1] we discussed the relationship between dc magnetization and ac susceptibility in a type-II superconductor. That work described how magnetic measurements provide information on hysteresis losses. In this paper, as in Ref. 1, we examine magnetization and susceptibility for longitudinal fields and no transport current. Here, however, we obtain the full-penetration fields, H_p, directly from the hysteresis loops rather than estimate H_p from measurements of critical current density, J_c. Also, we derive an expression for the reversible susceptibility, χ_{rev}, rather than using the experimental susceptibility, χ_{dc}, as an approximation. A superconducting wire whose low-field magnetization approached a reversible curve was selected for study.[2] Several minor hysteresis loops were obtained in addition to the major loop. The susceptibility curves were more nearly reversible and virtually independent of frequency, as expected from theory.

Table 1. Characteristics of Nb-Ti Wire

Cross section bare wire: 0.63 × 0.88 mm
Twist length: 1.7 cm
Cu/Nb-Ti volume ratio: 0.91
Number of filaments: 240
Filament radius: 19.3 μm
Density of Nb-Ti alloy: 6.20 g/cm^3

EXPERIMENT

The magnetization measurements were made with a vibrating-sample magnetometer (VSM) at 4 K. Magnetization was computed as magnetic moment per unit volume of Nb-Ti. The volume of the Cu matrix was not included.

It is useful to compare the advantages of the VSM method vis-à-vis the popular integration method of Fietz.[3] The VSM method (1) is useful for small samples, (2) is a dc measurement, not sensitive to coupling losses, (3) does not require precise pick-up coil balance when the applied field is stepped, and (4) is not subject to integrator drift. The integration method (1) measures frequency dependences, (2) detects flux jumps, and (3) is easily adaptable to measurements with transport current.

The experimental methods are more fully described in Ref. 1. The sample in this study is different and its length is 3.0 rather than 1.5 cm. The purpose of a longer sample was to avoid significant end effects. The characteristics of the wire are given in Table 1. This is the same wire as sample 8 in Ref. 2.

DC HYSTERESIS LOOP

Full-Penetration Field

The major and minor hysteresis loops are shown in Fig. 1. The full-penetration field, H_p, a function of applied field, H, may be estimated directly for each minor loop.[2] As the loops are traversed, the filaments go from full penetration in one direction to full penetration in the other direction. Therefore, at a high-field end of a loop, H_p is approximately one-half the field required to reverse the magnetization. The reversal field, $2H_p$, for the major loop is shown in Fig. 1.

The well-known Kim model for critical current density is[4]

$$J_c(H) = J_c(0)/(1+H/H_k) , \qquad (1)$$

where $J_c(0)$ and H_k are constants. In the critical-state model, for a field applied axially,

$$H_p = J_c r , \qquad (2)$$

where r is the filament radius. We did a linear least-squares fit of each loop's H_p to the expression

$$H_p(H) = H_p(0)/(1+H/H_k) , \qquad (3)$$

where $H_p(0)$ is a constant equal to $J_c(0)r$. The fit was excellent. We obtained $H_p(0)$ = 140 kA/m (1.76 kOe) and H_k = 1.33 MA/m (16.7 kOe).

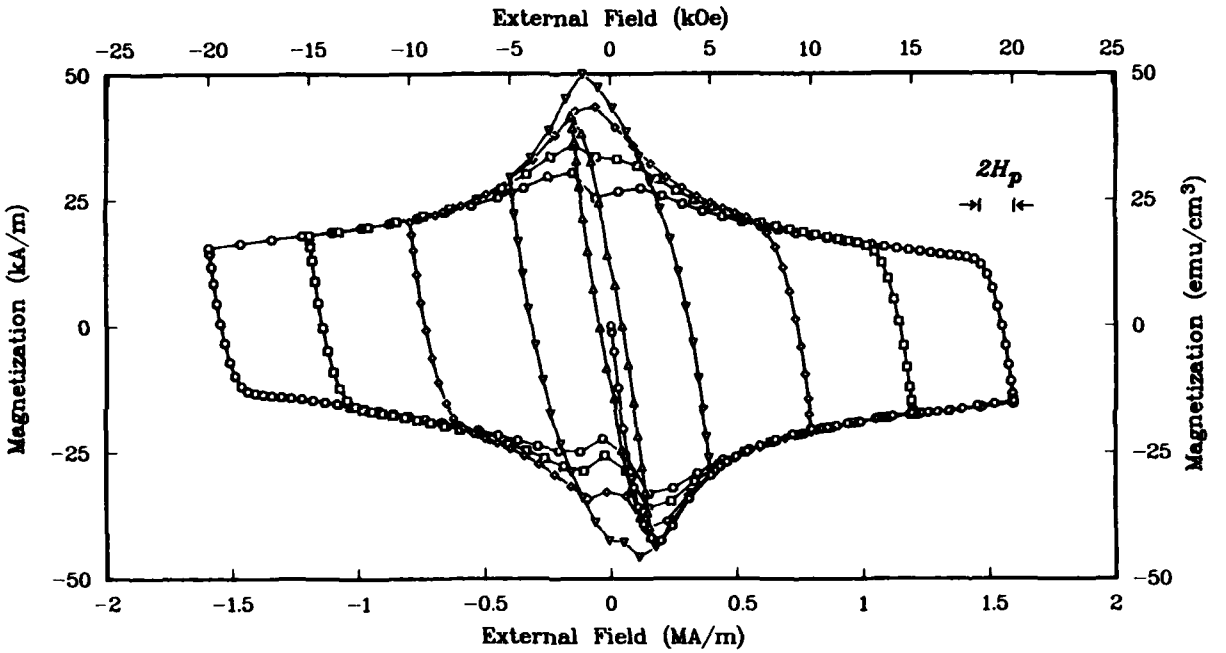

Fig. 1. Major and minor hysteresis loops for a multifilamentary Nb-Ti superconductor. DC magnetization is plotted vs. longitudinal applied field.

Table 2. Comparison of Losses Obtained from Eq. 4 and Loop Area.

H_0 (kA/m)	H_p	Eq. 4 (kJ/m^3)	Area (kJ/m^3)
1591	63	165	159
1194	74	143	136
796	87	110	105
398	108	62	58

Hysteresis Loss

For the case when the peak applied field, H_0, is greater than H_p, Carr derived an expression for the loss, assuming J_c to be spatially constant and field independent in the London-Bean approximation.[5] In SI units,

$$W = (4\mu_0 H_0 H_p/3)(1-H_p/2H_0) \quad . \tag{4}$$

Clearly H_0 is much larger than H_p for the loops in Fig. 1. Losses calculated by numerically integrating the loops are compared in Table 2 to losses obtained from Eq. 4. They agree to within 6%.

REVERSIBLE SUSCEPTIBILITY χ_{rev}

An exact equation for the ideal, reversible magnetization-versus-field curve of a type-II superconductor, $H > H_{c1}$, is not obtainable in analytic form. The usual procedure is to divide the field into three regions: immediately above H_{c1} ($H_{c1} \lesssim H$), the middle region ($H_{c1} < H < H_{c2}$), and immediately below H_{c2} ($H \lesssim H_{c2}$), and make judicious approximations.

One tractable case is $H_{c1} < H < H_{c2}$, when the separation between flux vortices is larger than the coherence length, ξ, but much smaller than the penetration depth, λ. Thus the Ginzburg-Landau parameter $\kappa \equiv \lambda/\xi$ is much greater than 1. For Nb-Ti at 4 K,[6] $\lambda \approx 394$ nm and $\xi \approx 5$ nm, and this case is applicable. To first order, the magnetization as a function of magnetic field strength M(H) is[7]

$$M = (\phi_0/8\pi\mu_0\lambda^2)\{\ln[4\pi\mu_0(H-H_{c1})\lambda^2/\phi_0] + \alpha\} - H_{c1} \quad , \tag{5}$$

where ϕ_0 is the magnetic flux quantum $= h/2e = 2.068 \times 10^{-15}$ Wb ($T \cdot m^2$) and α is a constant on the order of unity. The functional dependence of M(H) can be seen by dropping the α term and using the relationship[8]

$$H_{c1} = (\phi_0/4\pi\mu_0\lambda^2)\ln(\lambda/\xi) \quad . \tag{6}$$

Thus,

$$M = -(\phi_0/8\pi\mu_0\lambda^2)\ln[\phi_0/4\pi\mu_0(H-H_{c1})\xi^2] \quad . \tag{7}$$

The volume magnetic susceptibility $\chi = dM/dH$ can be obtained from either Eq. 5 or 7 and is simply

$$\chi = \phi_0/8\pi\mu_0(H-H_{c1})\lambda^2 \quad . \tag{8}$$

We take this χ to be equal to the ideal reversible susceptibility χ_{rev} in the range $H_{c1} < H < H_{c2}$. For $H < H_{c1}$, $\chi_{rev} = -1$. χ_{rev} represents the susceptibility under conditions of thermodynamic equilibrium.

Our goal is to obtain numerical values for χ_{rev} for our wire. The differential slope of the third-quadrant branch of the major magnetization curve (Fig. 1), from 0.2 to 1.6 MA/m (2.5 to 20 kOe), was fit to Eq. 8 using linear least squares. While this portion of the magnetization curve itself is not reversible, we expect that its slope will simulate χ_{rev}. For the adjustable parameters H_{c1} and λ, we obtain 92 kA/m (1 kOe) and 78 nm, respectively. These values are not too unreasonable, though this fit risks overestimating H_{c1} with values closer to $H_p(0)$. Substituting into Eq. 8 we get χ_{rev} for this wire for $H_{c1} < H < H_{c2}$ (SI units):

$$\chi_{rev} = 10772/(H-91751) \ . \qquad (9)$$

This equation will be used in the next section to calculate χ' and χ''. An alternate approach would be to use textbook values of H_{c1} and λ in Eq. 8.[9] This would give slightly different values of χ' and χ'' for $H \geq H_{c1}$. For larger fields, the differences are negligible.

MEASURED AND IDEAL χ' AND χ''

The real and imaginary components of susceptibility, χ' and χ'', were measured as functions of frequency (10, 100 and 1000 Hz), sinusoidal ac field amplitude, h [11 and 56 kA/m (140 and 700 Oe)], and dc bias field, H [0 - 1.6 MA/m (0 - 20 kOe)]. The susceptibilities were independent of frequency to within 3%. Since χ'' is a measure of the losses and hysteresis is known to be frequency independent, bulk hysteresis is probably the primary loss mechanism. Frequency-dependent eddy-current and coupling losses are likely insignificant for this sample.

Figures 2 and 3 show χ' and χ'' measured at 10 Hz. The initial and decreasing-field branches are plotted. Some irreversibility may be seen. In Fig. 3, h is on the order of H_p. As shown by Clem,[10] χ' and χ'' as functions of H may be predicted from h, H_p, and χ_{rev}. For our cases, $h < H_p$, the equations are:[1,10]

$$\chi' = (1+\chi_{rev})(h/H_p - 5h^2/16H_p^2) - 1 \ , \qquad (10)$$

$$\chi'' = (1+\chi_{rev})(4h/H_p - 2h^2/H_p^2)/3\pi \ . \qquad (11)$$

Using the expressions for H_p and χ_{rev} (Eqs. 3 and 9), we computed the theoretical curves of χ' and χ'' for this wire for ac field amplitudes of 11 and 56 kA/m (140 and 700 Oe). They are shown in Figs. 4 and 5. They compare quite favorably with the actual curves in Figs. 2 and 3. For $H < H_{c1}$, $\chi' = -1$ and $\chi'' = 0$. There are discontinuities at H_{c1}, as expected. In the actual curves these are rounded owing to flux pinning.

CONCLUSION

DC magnetization curves and measurements of complex susceptibility provide information on hysteretic losses in multifilamentary superconductors such as Nb-Ti. These measurements may be performed on small samples. Interpretation of the data yields information on full-penetration field, critical current density, lower critical field, and penetration depth. The frequency independence of susceptibility suggests bulk hysteresis as the primary loss mechanism.

ACKNOWLEDGMENT

This work was sponsored by the Air Force Office of Scientific Research.

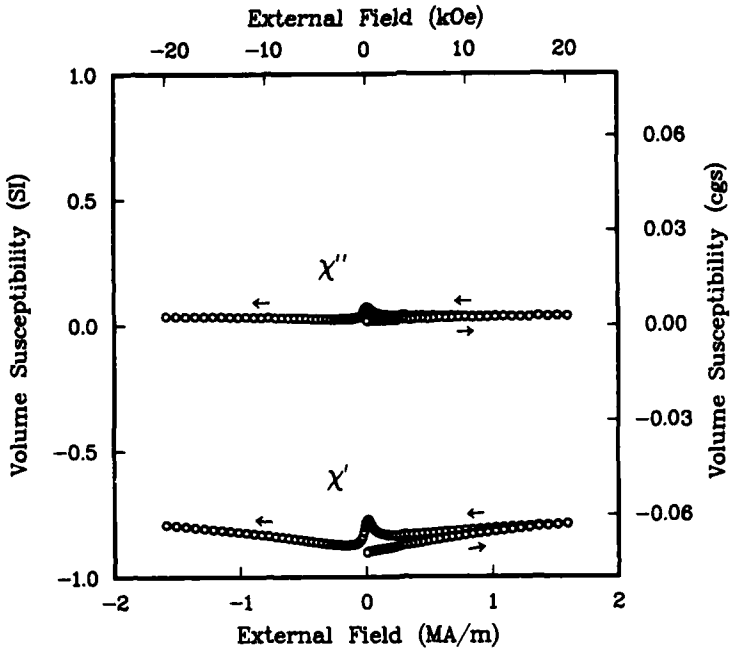

Fig. 2. Complex ac susceptibility as a function of dc bias field. The ac field amplitude is 11 kA/m (140 Oe) at 10 Hz.

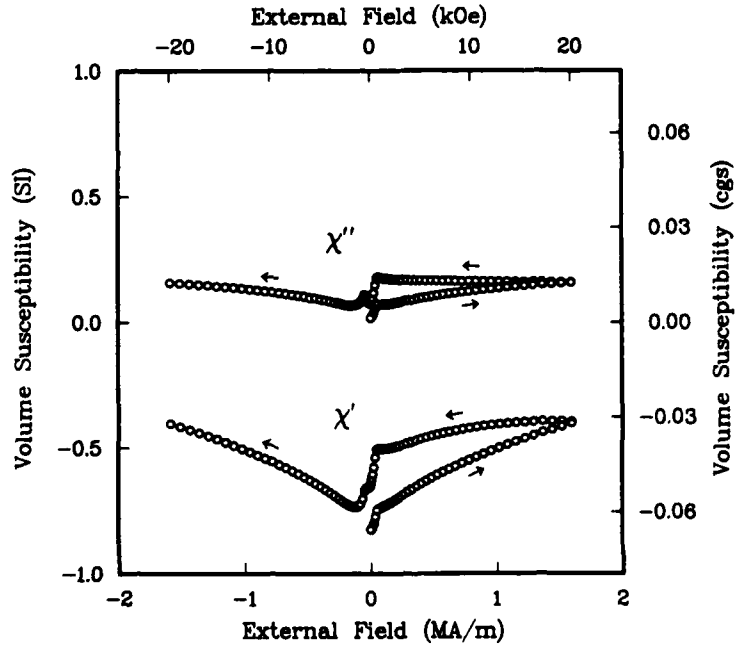

Fig. 3. Complex ac susceptibility as a function of dc bias field. The ac field amplitude is 56 kA/m (700 Oe) at 10 Hz.

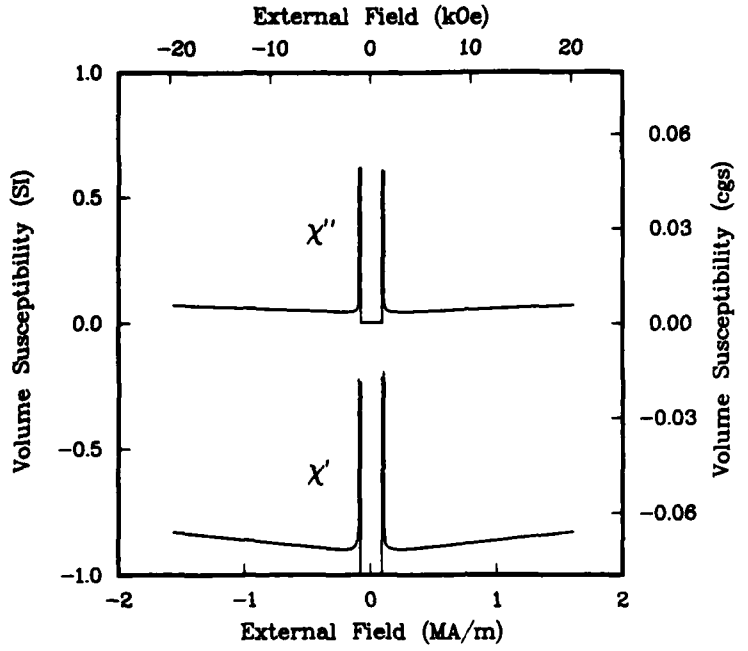

Fig. 4. Theoretical complex susceptibility vs. dc bias field for an ac field amplitude of 11 kA/m (140 Oe).

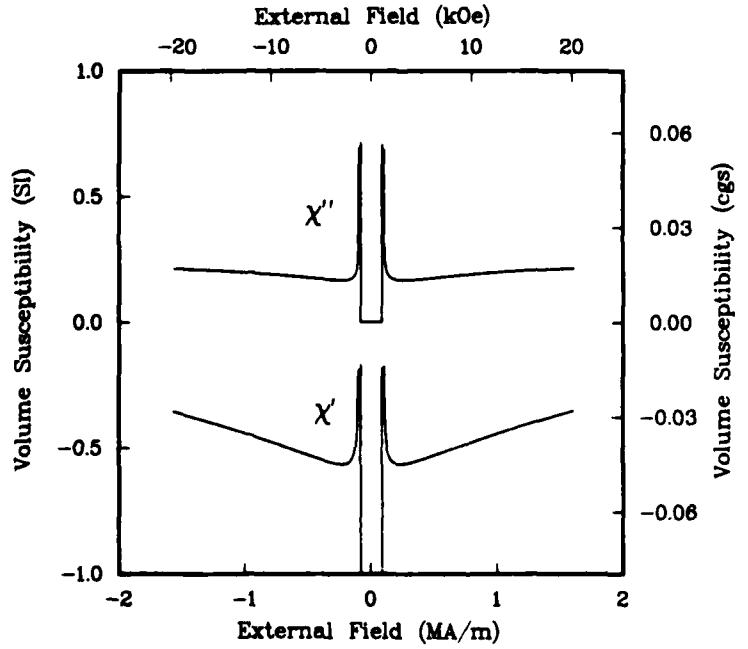

Fig. 5. Theoretical complex susceptibility vs. dc bias field for an ac field amplitude of 56 kA/m (700 Oe).

REFERENCES

1. R. B. Goldfarb and A. F. Clark, Magnetic hysteresis and complex susceptibility as measures of ac losses in a multifilamentary NbTi superconductor, IEEE Trans. Magn. MAG-21:332 (1985).
2. R. B. Goldfarb and A. F. Clark, Hysteretic losses in Nb-Ti superconductors, J. Appl. Phys. 57:3809 (1985).
3. W. A. Fietz, Electronic integration technique for measuring magnetization of hysteretic superconducting materials, Rev. Sci. Instrum. 36:1621 (1965).
4. Y. B. Kim, C. F. Hempstead, and A. R. Strnad, Magnetization and critical supercurrents, Phys. Rev. 129:528 (1963).
5. W. J. Carr, Jr., "AC Loss and Macroscopic Theory of Superconductors," Gordon and Breach, New York (1983), p. 70.
6. M. R. Beasley and T. P. Orlando, cited by R. J. Donnelly, in: "Physics Vade Mecum," H. L. Anderson, ed., American Institute of Physics, New York (1981), ch. 7, p. 121.
7. A. L. Fetter and P. C. Hohenberg, in: "Superconductivity," R. D. Parks, ed., Marcel Dekker, New York (1969), ch. 14, p. 838.
8. A. L. Fetter and P. C. Hohenberg, in: "Superconductivity," R. D. Parks, ed., Marcel Dekker, New York (1969), ch. 14, p. 843.
9. Cf. $H_{c1} \approx 8$ kA/m (100 Oe), in: A. K. Ghosh and W. B. Sampson, Magnetization and critical currents of NbTi wires with fine filaments, paper DZ-7, this conference.
10. J. R. Clem, "AC Losses in Type-II Superconductors," Ames Lab. Tech. Rept. IS-M 280, Iowa State University, Ames (1979), pp. 23-24.

Eleventh International Cryogenic Engineering Conference - ICEC 11
West Berlin - April 1986
Paper 09-4

LOSSES IN A Nb-Ti SUPERCONDUCTOR AS FUNCTIONS OF AC FIELD AMPLITUDE AND DC TRANSPORT CURRENT

M. Dragomirecky, J.V. Minervini, J.W. Ekin, R.B. Goldfarb, and A.F. Clark

National Bureau of Standards, Boulder, Colorado 80303, USA

Hysteretic shielding losses and transport losses were measured in a multifilamentary Nb-Ti superconducting coil as functions of transverse ac field amplitude and dc transport current. The conductor was biased with a dc field. There was significant agreement with the predictions of Minervini's two-dimensional theoretical model.

INTRODUCTION

AC losses for the case of current-carrying conductors in transient applied magnetic fields are of importance in practical applications. The theory for the one-dimensional slab model is well known and a few experimental studies have been made. Predominant among these is the work of Ogaswara, et al. [1-4]. For multifilamentary conductors, they emphasize the dependence of loss on the rate of change of the field. Their field amplitudes were rather large, on the order of 200 kA/m (2.5 kOe). Ciazynski also examined the dependence of hysteresis and transport losses on the sweep rate of the applied field. The analysis was in terms of an equivalent electrical network [5]. Bruzzone and Kwasnitza discussed the dependence of the hysteresis loss on the ratio of ac field amplitude to full-penetration field [6]. References [1-6] are primarily concerned with coupling losses in multifilamentary conductors. De Reuver et al. [7] recently reported measurements of losses in conductors carrying dc transport current in a transverse ac field. They analyzed their data in terms of the slab model and found qualitative agreement.

The first complete two-dimensional analysis for a cylindrical conductor with a transport current in a transverse ac field was presented by Minervini in 1981 [8]. The theory is based on the London-Bean approximation where the critical current density, J_c, is independent of field, H. Ignoring eddy-current and coupling losses (for low-frequency ac fields), the total ac loss can be separated into two components. (1) Shielding hysteresis loss occurs in the outer volume of the superconductor filament not occupied by transport current. (2) Transport loss occurs owing to flux motion through the central portion of the superconductor filament when the shielding region is saturated with shielding currents. The shielding hysteresis loss, W_s, and transport loss, W_t, as functions of transport current density, J, are shown in Figs. 1 and 2 [8]. The total loss would be equal to the sum of W_s and W_t. Curves are shown for different ac field amplitudes, h. The energies W_s and W_t are normalized to W_0, J is normalized to J_c, and h is normalized to $H_p(0)$, where, for filaments of diameter d,

$$H_p(0) = d\, J_c / \pi \tag{1}$$

is the full-penetration field for zero transport current (J = 0), and

$$W_0 = 4\, \mu_0\, H_p^2(0) / 3 \tag{2}$$

is the volume energy density when $h = H_p(0)$ and $J = 0$ [9]. $H_p(J)$ is a monotonically decreasing function of J. In this paper we report measurements of shielding hysteresis loss and transport loss that were made in an effort to test the two-dimensional model. The results are in good agreement with the model. More experimental data are needed to adequately determine the detailed shape of the curves.

EXPERIMENT AND RESULTS

A multifilamentary Nb-Ti conductor was noninductively wound on a coil form. Inner and outer balanced pick-up coils were wound coaxially. The sample was immersed in liquid helium. It was exposed to a 3-MA/m (40-kOe) dc bias field. The purpose of the bias field was primarily to operate on the relatively flat portion of the J_c-versus-H curve, where, as assumed in the London-Bean approximation, J_c is not a strong function of H [10]. A secondary purpose of the bias field was to reduce J_c to a value more accessible in the laboratory and to operate under conditions similar to those in practical applications.

The wire selected for study had a diameter of 0.635 mm, 180 filaments 30 um in diameter, and a copper-to-superconductor volume ratio of 1.50. This wire was the same as sample 4 in Ref. [11]. The sample was 18 m long, wound in two layers of 72 and 74 turns. The critical current while in the bias field was 310 A, giving a filament J_c of 2.44×10^9 A/m^2 at 3 MA/m (40 kOe). $H_p(0)$ was 2.33×10^4 A/m (290 Oe) and W_0 was 910 J/m^3.

Data were acquired with a computer-controlled, four-channel digital recording oscilloscope. The voltage waveform of the pick-up coil was integrated with respect to time to give magnetization, which was plotted as a function of the ac-field waveform. The resulting hysteresis loop was numerically integrated to get the shielding hysteresis loss. The energy for the loss was provided by the ac-field power supply.

The magnetization axis was calibrated by noting that the maximum magnetization value for ac fields greater than $H_p(0)$ for zero transport current is $2H_p(0)/3$ [9]. An alternate calibration would be to use the initial susceptibility in zero bias field with an ac field amplitude less than the lower critical field, H_{c1}. However, the external susceptibility when the field is applied along the axis of the sample coil depends on the effective demagnetization factor, a function of how tightly the coil is wound [12]. This could not be determined accurately.

Transport loss was numerically computed as the integral, over two complete cycles, of the product of sample voltage and transport current. The energy for the transport loss was provided by the transport-current power supply.

The frequency of the ac field was 1 Hz, far below the frequency for which coupling currents or eddy currents become important. Unlike in earlier studies [1-7], the frequency of the ac field was not a variable. The experimental set-up is shown in Fig. 3. Particular care was taken to avoid ground loops and thermal voltages. Very low-noise (< 3 uV) preamplifiers were used. Any dc offsets of the amplifiers were subtracted from the measured waveforms. The results are shown in Figs. 4 and 5.

DISCUSSION

Generally speaking, this was a difficult experiment. The agreement of the experimental results (Figs. 4 and 5) with the theory (Figs. 1 and 2) is fairly good. The need for more data to fill-in the curves is noted.

For the case $J = 0$ and $h \geq H_p(0)$, the theoretical expression for W_s/W_0 [8] reduces to

$$W_s/W_0 = 2h/H_p(0) - 1 \ . \qquad (3)$$

Thus, the consistency of the values for $h/H_p(0)$ and W_s/W_0 ($J = 0$) in Fig. 4 can be evaluated with reference to Fig. 1. For example, the curve for $h/H_p(0) = 1$ should intercept the W_s/W_0 axis at unity.

The theoretical curves for the one-dimensional slab model are only qualitatively similar to those for the two-dimensional cylindrical model. However, when the data

were normalized to the values of $H_p(0)$ and W_0 for the slab model and compared to the theoretical slab-model curves, the quantitative agreement was poor. For shielding loss, the measured values were greater by a factor of about 2. For transport loss, the measured curves had a different curvature. Furthermore, the total-loss curves ($W_s + W_t$) for our data are in excellent quantitative agreement with the theoretical total-loss curves for the two-dimensional model [8] but in poor agreement with the theoretical curves for the slab model [1-4,7].

Though our data do not include large ac field amplitudes, we consider this case for the purpose of comparison to the high-field work of others. When $h/H_p(0) \gg 1$, $W_s/W_0 = 2h/H_p(0)$. In this limit, from Eqs. 2 and 3,

$$W_s = 8\ \mu_0\ H_p(0)\ h\ /\ 3\ , \tag{4}$$

in agreement with Carr's derivation [13].

CONCLUSION

The two-dimensional cylindrical model seems to be better than the one-dimensional slab model for analyzing shielding hysteresis losses and transport losses in multifilamentary conductors with round filaments.

ACKNOWLEDGEMENT

This work was sponsored by the Air Force Office of Scientific Research.

REFERENCES

1 Ogaswara, T., Takahashi, Y., Kanbara, K., Kubota, Y., Yasohama, K., and Yasukochi, K., 'Alternating field losses in superconducting wires carrying dc transport current. Part 1: single core conductors'. Cryogenics, vol. 19 (1979), pp.736-740.

2 Ogaswara, T., Takahashi, Y., Kanbara, K., Kubota, Y., Yasohama, K., and Yasukochi, K., 'Transient field losses in multifilamentary composite conductors carrying dc transport currents'. Cryogenics, vol. 20 (1980), pp.216-222.

3 Ogaswara, T., Takahashi, Y., Kanbara, K., Kubota, Y., Yasohama, K., and Yasukochi, K., 'Alternating field losses in superconducting wires carrying dc transport current. Part 2: multifilamentary composite conductors'. Cryogenics, vol. 21 (1981), pp.97-101.

4 Ogaswara, T., Itoh, M., Kubota, Y., Kanbara, K., Takahashi, Y., Yasohama, K., and Yasukochi, K., 'Transient field losses in multifilamentary composite conductors carrying transport currents'. IEEE Trans. Magn., vol. MAG-17 (1981), pp.967-970.

5 Ciazynski, D., 'Effect of a transport current on the losses of a superconducting composite under fast changing magnetic field'. IEEE Trans. Magn., vol. MAG-21 (1985), pp.169-172.

6 Bruzzone, P. and Kwasnitza, K., 'Scaling law for filamentary superconductor hysteresis losses in superimposed dc and ac magnetic fields'. J. Physique Colloq. C1, vol. 45 (1984), pp.483-487.

7 De Reuver, J.L., Beunk, H.D., Roovers, A.J.M., and Van der Klundert, L.J.M., 'AC field losses in a dc current-carrying conductor containing one layer of NbTi filaments'. Intl. Conf. Magnet Tech., MT-9, Marinucci, C. and Weymuth, P., eds., Swiss Inst. Nucl. Res., Zurich (1985), pp.501-504.

8 Minervini, J.V., 'Two-dimensional analysis of ac loss in superconductors carrying transport current'. Advances in Cryogenic Engineering (Materials), Vol. 28, Reed, R.P. and Clark, A.F., eds., Plenum, New York (1982), pp.587-599.

9 Pang, C.Y., McLaren, P.G., and Campbell, A.M., 'Losses in superconducting cylinders in transverse fields'. Intl. Cryo. Engr. Conf., Vol. 8, Rizzuto, C., ed., IPC Sci. and Tech. Press, Surrey, England (1980), pp.739-743.

10 Carr, Jr., W.J., AC Loss and Macroscopic Theory of Superconductors, Gordon and Breach, New York (1983), p.55.

11 Goldfarb R.B. and Clark, A.F., 'Hysteretic losses in Nb-Ti superconductors'. J. Appl. Phys., vol. 57 (1985), pp.3809-3811.

12 Sumiyoshi, F., Irie, F., and Yoshida, K., 'The effect of demagnetization on the eddy-current loss in a single-layered multifilamentary superconducting coil'. J. Appl. Phys., vol. 51 (1980), pp.3807-3811.

13 Carr, Jr., W.J., AC Loss and Macroscopic Theory of Superconductors, Gordon and Breach, New York (1983), p.67.

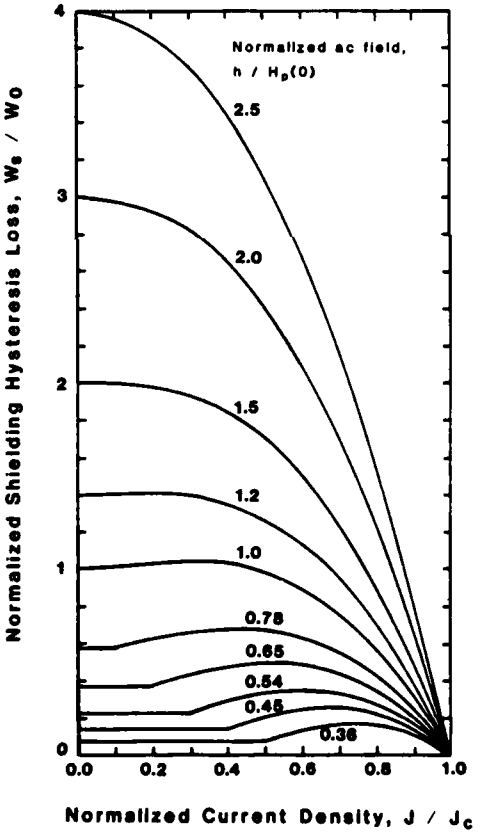

Fig. 1 Theoretical shielding hysteresis loss for different ac fields [8].

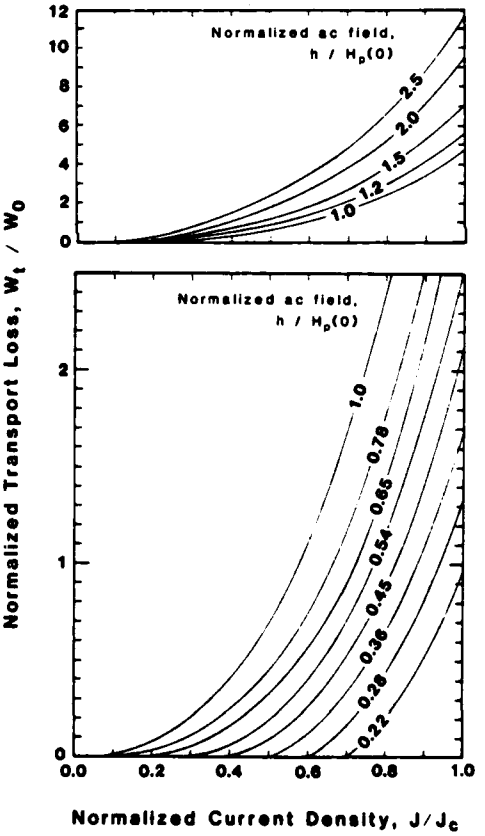

Fig. 2 Theoretical transport loss for different ac fields [8].

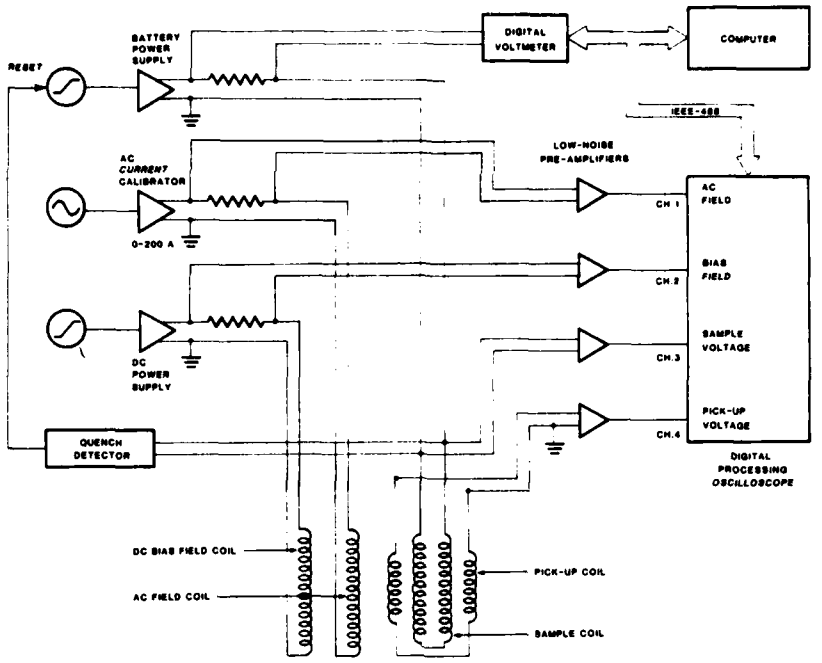

Fig. 3 Experiment for measuring shielding hysteresis loss and transport loss. The coils are immersed in liquid helium.

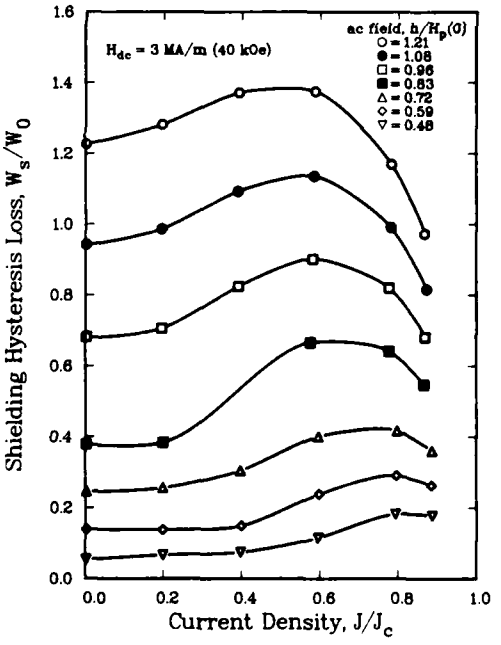

Fig. 4 Experimental shielding hysteresis loss for different ac fields.

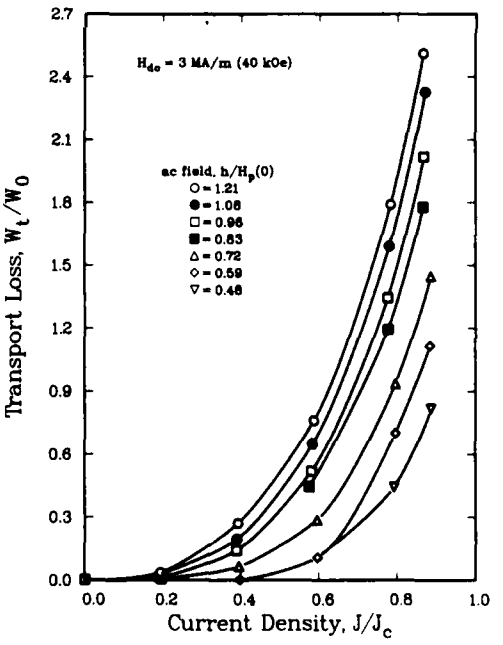

Fig. 5 Experimental transport loss for different ac fields.

HYSTERESIS LOSSES IN FINE-FILAMENT INTERNAL-TIN SUPERCONDUCTORS

R. B. Goldfarb and J. W. Ekin
Electromagnetic Technology Division
National Bureau of Standards
Boulder, Colorado 80303

ABSTRACT

Hysteresis losses were measured on a series of fine-filament Nb_3Sn superconductors made by the internal-tin process. Hysteresis was measured as a function of filament diameter and interfilament separation using a vibrating-sample magnetometer in transverse field. Losses were greater than expected from the critical-state model that expresses loss as a function of filament diameter. Micrographs of the reacted wire cross sections showed some interfilament bridging for all wires. This gave rise to effective filament diameters that were greater than actual diameters. The critical interfilament separation, above which the losses would be expected to follow the critical-state model, was determined.

INTRODUCTION

Fine-filament superconductors are of interest in ac-loss studies because, according to the critical-state model, hysteresis loss is proportional to filament diameter. Thus, one would expect that wires composed of fine filaments would exhibit small losses. In this study we used a vibrating-sample magnetometer in transverse magnetic field to measure the dc hysteresis loss for a series of Nb_3Sn superconductors made by the internal-tin process. There was no transport current. Filament diameter and edge-to-edge interfilament separation were systematically varied to determine whether filament coupling caused larger-than-expected hysteresis losses. Such magnified losses may be

expressed in terms of an effective filament diameter that is greater than the actual filament diameter. The effective diameter is deduced from the hysteresis loss using the critical-state model.

There has been some previous work on hysteresis losses in fine-filament superconductors. Dubots et al. compared measured and calculated hysteresis in Nb-Ti conductors with filament diameters ranging from 10 to 0.1 μm [1]. They found that, for diameters smaller than 1 μm, effective filament diameters remained about 1 μm. Information on interfilament separation was not given. Carr and Wagner attributed the asymmetrical hysteresis curve they observed in Nb-Ti with 1.6-μm filament diameter to relatively large surface currents [2]. Ghosh and Sampson studied fine-filament Nb-Ti with filament diameters in the range 1-5 μm [3]. They note that, for diameters less than 3 μm, the magnetization (and therefore hysteresis loss) is larger than expected from the critical-state model. They attribute this to degradation of the magnitudes of critical current owing to filament necking or damage.

In this paper we show that certain Nb_3Sn internal-tin conductors with filament diameters smaller than 5 μm have effective filament diameters greater than expected from the critical-state model. The ratio of effective to actual Nb_3Sn filament diameters appears to be a linear function of interfilament separation. The slope of the line is a function of the local area ratio of matrix material to Nb for each wire. The greater effective filament diameters appear to be a consequence of bridging between filaments.

SAMPLE PREPARATION AND MEASUREMENT

The multifilamentary Nb_3Sn wires used in this study were composed of subelements containing 150 filaments each. The array of subelements was surrounded by a tantalum diffusion barrier. Unreacted Nb_3Sn wires were wrapped

on the threads of size 10-24 stainless steel screws. The thread pitch was such that the windings were not in contact with each other. The screws had been previously oxidized to prevent the wires from sticking to the screws. The internal-tin-process wires were reacted in vacuum, with cold ends out of the furnace, according to the following schedule: 1 day at 340°C, 4 days at 580°C, and 4 days at 700°C. This schedule is adequate to fully react the wires for the filament diameters in this study [4]. The residual tin content of each wire after reaction was estimated by the manufacturer to be 8 wt.%.

After reaction, the wire coils were unscrewed from the stainless screws and the long ends cut off. Each coil was about 1.3 cm in height. The wire volumes were measured using Archimedes' principle. The wire diameter was the same for each sample, 0.681 mm. Thus, the wire length for each coil was obtained.

The average Nb-filament diameters before reaction and number of filaments in each sample were provided by the manufacturer. The reacted filament diameters and total volume of Nb_3Sn in each coil were calculated based on a presumed increase of 38% in filament cross-sectional area after reaction [5]. Local area ratios of matrix to Nb were determined by the manufacturer from the arrangement of the Nb rods in the billets before drawing: the Nb may be thought of as enclosed by adjacent hexagons and the cross-sectional areas of Nb and matrix material measured. The average center-to-center filament distance, s, may be determined from the local area ratio, L, and Nb filament diameter, d, by the equation

$$L = (2\sqrt{3}/\pi)(s/d)^2 - 1 \ . \qquad (1)$$

The edge-to-edge Nb separation is simply s - d.

Table 1 gives relevant parameters for the six samples. Note that Nb diameter plus Nb separation equals Nb_3Sn diameter plus Nb_3Sn separation.

Both sums are equivalent to the center-to-center filament distance (not shown). The matrix-to-Nb local area ratios of 1.5 and 1.8 correspond to area ratios for reacted Nb_3Sn of 1.0 and 1.2, respectively.

Magnetic moment was measured at 4.2 ± 0.2 K with a vibrating-sample magnetometer in the axis of the coil (i.e., field transverse to the wire if we ignore thread pitch of about 5.5°). Maximum applied field was 1.6 MA/m (20 kOe). There was no transport current and the coils were open-circuited. Magnetization was computed as magnetic moment per unit volume of Nb_3Sn (i.e., not including the volume of the matrix material). Magnetization was plotted versus external (applied) magnetic field. A typical magnetic hysteresis loop for one of the samples (sample 18) is shown in Fig. 1.

RESULTS

Hysteresis loss was computed by numerically integrating the loop area, ignoring the initial branch. According to the critical-state model, for transverse field geometry [6]:

$$W = 8 J_c d_{eff} \mu_0 H_0 / 3\pi \qquad \text{(SI units)} \qquad (2)$$

Thus, an effective filament diameter, d_{eff}, may be defined that is a function of the hysteresis loss, W, for a maximum applied field, H_0. Since we did not have data for the critical current density, J_c, at 1.6 MA/m (20 kOe), we deduced these J_c based on the critical current of each wire measured at 6.4 MA/m (80 kOe) together with the total Nb_3Sn cross-sectional area and the measured value of the full-penetration field, H_p, at 1.6 MA/m (20 kOe). J_c, H_p, and filament diameter, d, are related according to the critical-state model [6]:

$$H_p = d J_c / \pi \qquad \text{(SI units)} \qquad (3)$$

H_p may be obtained as one-half the field required to reverse the magnetization

[7]. From the hysteresis loops, H_p at 1.6 MA/m (20 kOe) is roughly 75 kA/m (940 Oe) for all the loops. This suggests a factor of 10 increase in J_c compared to measured J_c at 6.4 MA/m (80 kOe). Applying this factor of 10 to each conductor gives the values of J_c shown in Table 2. We then compute the effective filament diameters of the wires, and additionally, the ratio of the effective to actual Nb_3Sn filament diameters.

Optical and scanning-electron microscopy revealed that some of the filaments in each wire were not entirely isolated but were connected by "bridges". An example of this is shown in Fig. 2. Such filaments had typically lost their original hexagonal spacing and aligned themselves in rows in the process of wire drawing [8].

DISCUSSION

As shown in Fig. 3, the relationship between actual and effective Nb_3Sn diameters is not monotonic. However, some insight is obtained by plotting the ratio of effective to actual Nb_3Sn diameters versus Nb_3Sn interfilament separation (see Fig. 4). It appears that effective filament diameter is a function of both actual filament diameter and interfilament separation. Thus, loss per volume of Nb_3Sn superconductor is a function of both parameters.

Further refinement is possible by distinguishing among those conductors with the same matrix-to-Nb local area ratios. These are identified in Figs. 3 and 4 for the two ratios. We see in Fig. 3 that there is less of an increase in effective filament diameter for the conductors with the larger local area ratio. However, we note that, in Fig. 4, the abscissa (Nb_3Sn interfilament separation) is not independent of local area ratio (see Eq. 1). The apparently linear dependence of the effective-to-actual diameter ratio on interfilament separation has no physical significance.

A critical interfilament separation can be defined. It corresponds to the separation above which the hysteresis losses would depend on filament diameter as expected from the critical-state model. We determined the critical separation for reacted Nb_3Sn, as shown in Fig. 4, by linearly extrapolating the data to a unity value of effective-to-actual diameter ratio. The critical separation appears to be a function of the local area ratio. Critical values for the separation between reacted Nb_3Sn filaments were about 1.6 μm for an area ratio of 1.5 and about 2.0 μm for a ratio of 1.8. The corresponding critical values for the separation between unreacted Nb filaments were 2.4 and 1.5 μm, respectively.

CONCLUSION

Certain fine-filament superconductors made by the internal-tin process have effective filament diameters that are greater than actual filament diameters. The differences between effective and actual diameters increase as actual diameters decrease, the effect being more pronounced in those wires with the smaller local area ratio of matrix material to Nb. When the ratio of effective to actual diameters is plotted as a function of edge-to-edge interfilament separation, a more refined picture emerges. The diameter ratio increases linearly with decreasing interfilament separation for each local area ratio. The larger-than-expected effective filament diameters are likely due to interfilament bridging in these wires.

For the practical purpose of conductor design, a critical interfilament separation can be determined. It corresponds to the spacing above which the hysteresis loss would depend on filament diameter as expected from the critical-state model. The critical Nb_3Sn interfilament separation for the conductors used in this study was about 1.6 and 2.0 μm for matrix-to-Nb area ratios of

1.5 and 1.8, respectively. The critical separation is offered simply as a practical design parameter related to the critical-state model and for guidance in the manufacture of fine-filament internal-tin superconductors such as these.

ACKNOWLEDGMENTS

M. Suenaga made the high-field critical current measurements and generously shared samples of the unreacted wires. A. K. Ghosh astutely pointed out the importance of local area ratios. G. M. Ozeryansky provided valuable information on the physical characteristics of the wires. E. S. Pittman made the optical and scanning-electron micrographs. The wires were manufactured by Intermagnetics General Corporation [9]. The experimental work was sponsored by the Air Force Office of Scientific Research. Most of the results of this study were presented at the Fourth U.S.-Japan Workshop on High Field Superconducting Materials for Fusion, 1986. This workshop and the microanalysis were sponsored by the U.S. Department of Energy, Office of Fusion Energy.

REFERENCES

1. P. Dubots, A. Février, J. C. Renard, J. P. Tavergnier, J. Goyer, and Hoang Gia Ky, NbTi wires with ultra-fine filaments for 50-60 Hz use: Influence of the filament diameter upon losses, IEEE Trans. Magn. MAG-21, 177 (1985).

2. W. J. Carr, Jr. and G. R. Wagner, Hysteresis in a fine filament NbTi composite, in: "Advances in Cryogenic Engineering (Materials)," Vol. 30, A. F. Clark and R. P. Reed, eds., Plenum, New York (1984) p. 923.

3. A. K. Ghosh and W. B. Sampson, Magnetization and critical currents of NbTi wires with fine filaments, in: "Advances in Cryogenic Engineering (Materials)," Vol. 32, R. P. Reed and A. F. Clark, eds., Plenum, New York (1986) p. 809.

4. A. K. Ghosh, private communication.

5. G. M. Ozeryansky, private communication.

6. W. J. Carr, Jr., "AC Loss and Macroscopic Theory of Superconductors," Gordon and Breach, NY (1983) p. 67.

7. R. B. Goldfarb and A. F. Clark, Hysteretic losses in Nb-Ti superconductors, J. Appl. Phys. 57, 3809 (1985).

8. Evidence for interfilament bridging in these wires was first presented by A. K. Ghosh and W. B. Sampson in: "Magnetization studies of multifilamentary Nb_3Sn wires" at the Fourth U.S.-Japan Workshop on High Field Superconducting Materials for Fusion, 1986 (unpublished).

9. Certain commercial materials are identified to adequately specify the experimental study. In no case does such identification imply recommendation or endorsement by the National Bureau of Standards, nor does it imply that the material is the best available for the purpose.

TABLES

Table 1. Parameters for six Nb_3Sn multifilamentary superconductors.

Sample	Nb Diam. (μm)	Nb_3Sn Diam. (μm)	Local Area Ratio	Nb Sep. (μm)	Nb_3Sn Sep. (μm)	No. Fil.	Length (cm)	Vol. Nb_3Sn (mm^3)
3	4.2	4.9	1.5	2.1	1.4	2850	17.8	9.71
6	4.0	4.7	1.8	2.4	1.7	2850	17.3	8.55
9	3.0	3.5	1.5	1.5	1.0	5550	17.1	9.24
12	2.8	3.3	1.8	1.7	1.2	5550	17.0	8.01
15	2.3	2.7	1.5	1.2	0.8	9150	17.0	8.89
18	2.2	2.6	1.8	1.3	0.9	9150	16.8	8.04

Table 2. Hysteresis loss and effective filament diameters for Nb_3Sn.

Sample	Estimated J_c (GA/m^2)	W (MJ/m^3)	Eff. Nb_3Sn Fil. Diam. (μm)	Eff./Actual Diameter Ratio
3	49.4	0.870	10.46	2.12
6	50.6	0.714	8.37	1.78
9	50.6	1.369	16.05	4.55
12	54.3	0.885	9.67	2.94
15	53.8	1.419	15.66	5.80
18	51.9	0.805	9.20	3.56

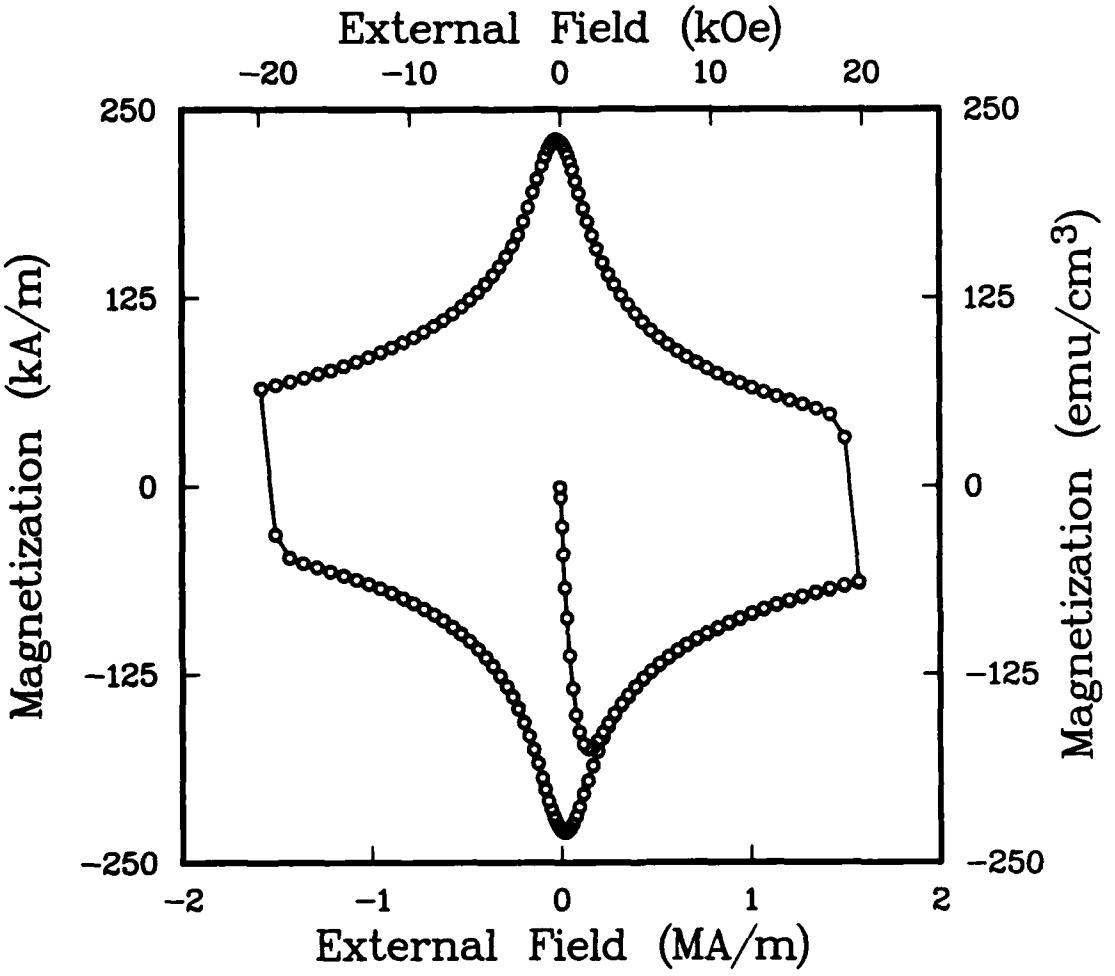

Figure 1. Typical hysteresis loop for a multifilamentary Nb_3Sn wire made by the internal-tin process (sample 18). Magnetization was computed as magnetic moment per unit volume of Nb_3Sn.

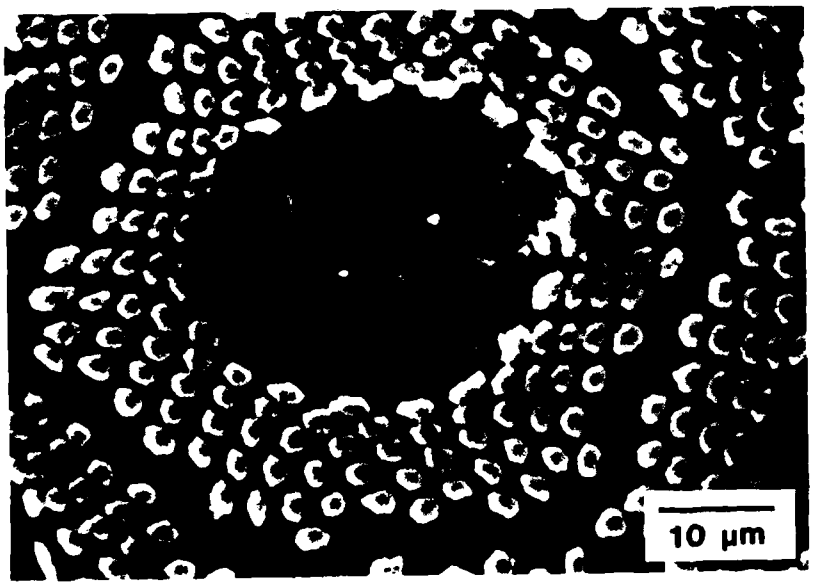

Figure 2. Typical scanning-electron micrograph showing some interfilament bridging (sample 18, center subelement).

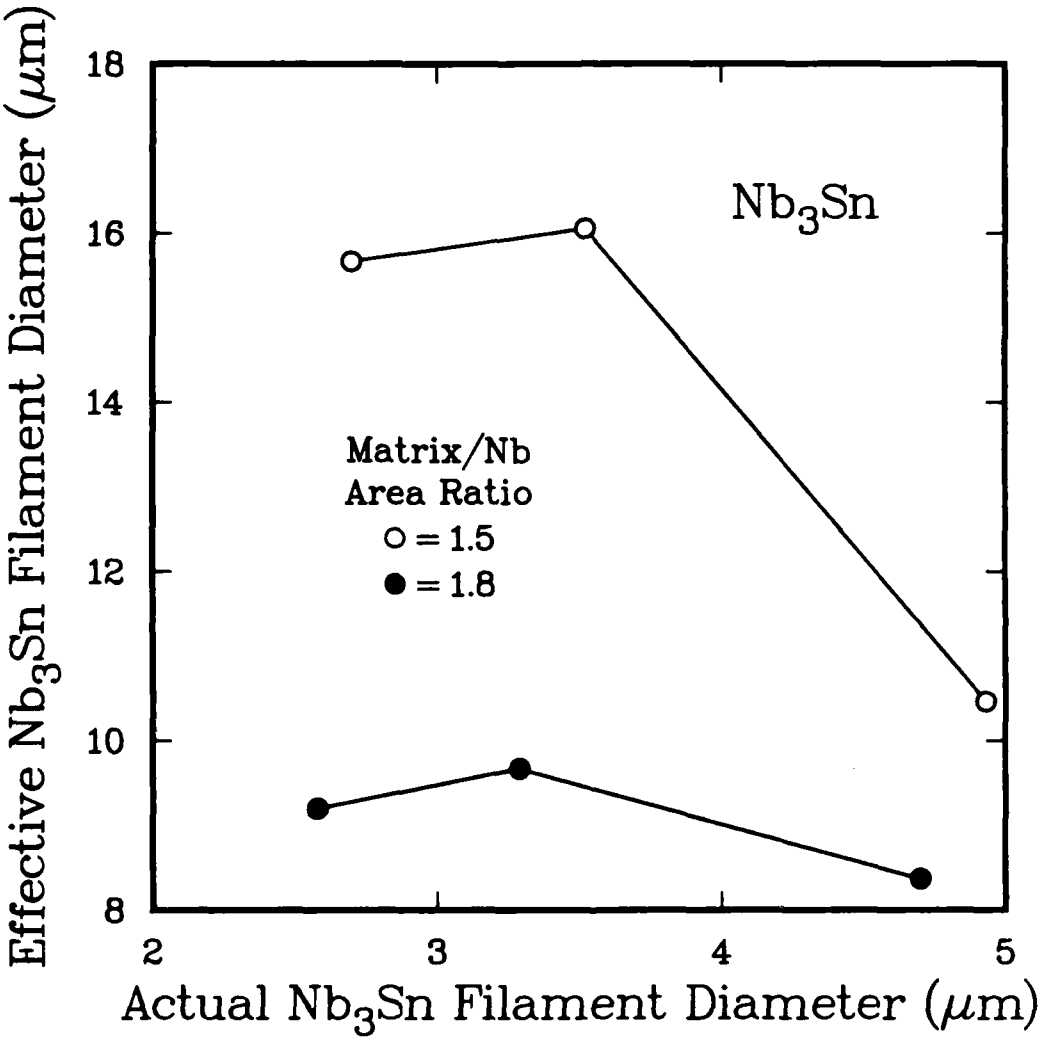

Figure 3. Effective filament diameter as a function of actual Nb_3Sn filament diameter for two local area ratios of matrix to Nb.

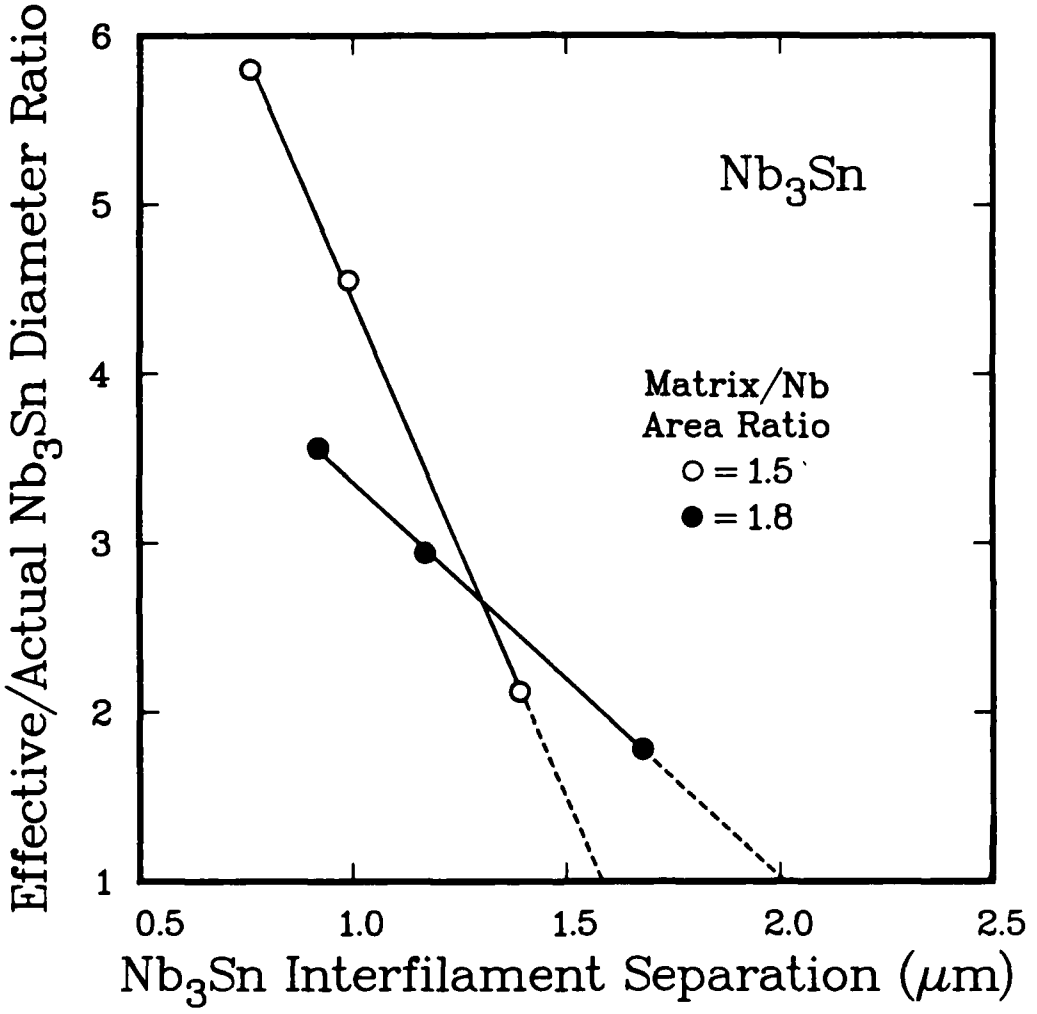

Figure 4. Ratio of effective to actual Nb_3Sn filament diameter as a function of Nb_3Sn interfilament separation for two local area ratios of matrix to Nb.

INTERNAL FIELDS IN MAGNETIC MATERIALS AND SUPERCONDUCTORS

R. B. Goldfarb
Electromagnetic Technology Division
National Bureau of Standards
Boulder, Colorado 80303

ABSTRACT

This paper reviews some of the concepts needed for the correct analysis of magnetization data, both for magnetic materials and superconductors. Demagnetization factors, initial susceptibilities, and hysteresis losses are discussed.

INTRODUCTION

Magnetization measurements have acquired an important function in the measurement of ac losses in superconductors. Many of the traditional analysis methods used for magnetic materials apply to superconductors with the assumption of perfect diamagnetism. Some refinement is necessary for type-II and multifilamentary superconductors.

DEMAGNETIZATION FACTORS

The magnetization curve characteristic of a magnetic material is obtained by plotting magnetization, M, versus internal field, H_{int}. H_{int} is obtained by correcting the external applied field, H_{ext}, by the demagnetization field, $H_{demag} = DM$, where D is the geometric demagnetization factor. In SI units,

$$H_{int} \equiv H_{ext} - DM \ . \qquad (1)$$

For a sphere, D = 1/3. For a long cylinder, with H_{ext} applied axially, D = 0; for H_{ext} applied transversely, D = 1/2. H_{int} corresponds to the field H in

the equation $B = \mu_0(H+M)$. H_{int} is sometimes referred to as the Maxwell field. Here we ignore any ac effects such as eddy currents.

INITIAL SUSCEPTIBILITIES

Often the initial slope of the magnetization curve is used for calibration of magnetometers. We define the internal susceptibility, χ_{int}, as dM/dH_{int} and the external susceptibility, χ_{ext}, as dM/dH_{ext}. Thus, from Eq. 1,

$$\chi_{int} = \chi_{ext} / (1 - D\,\chi_{ext}) , \qquad (2)$$

$$\chi_{ext} = \chi_{int} / (1 + D\,\chi_{int}) . \qquad (3)$$

Let us consider the case of a soft ferromagnet with a very large χ_{int}. In a small applied field H_{ext}, we would measure M such that, from Eq. 3, $\chi_{ext} = dM/dH_{ext} = 1/D$.

We can treat a simple type-I superconductor as a perfectly diamagnetic material: $\chi_{int} = -1$. In an applied field H_{ext}, from Eq. 3,

$$\chi_{ext} = dM/dH_{ext} = 1/(D-1) . \qquad (4)$$

Thus, for a sphere, $\chi_{ext} = -3/2$. For a long cylinder axially, $\chi_{ext} = -1$; transversely, $\chi_{ext} = -2$.

An interesting case is that of an infinitely thin sheet of finite dimensions. For H_{ext} normal to the surface, D = 1. From Eq. 4, χ_{ext}, and thus M, will approach infinity. While this seems unphysical at first, we note that M is calculated as magnetic moment per unit volume, V. M gets infinitely large only as V approaches zero. Furthermore, for $H_{ext} > 0$, flux immediately begins to penetrate the sheet in this "intermediate" state; full penetration occurs at $H = H_c$, the critical field.

For these cases, we plot M versus H_{ext} in Fig. 1 [1]. Note that M versus H_{int} would be characteristic of the material, independent of geometry. The plot of M versus H_{int} would be the same as that for the axial cylinder (D = 0).

The same initial χ_{int} would be obtained for a type-II superconductor. The lower critical field, H_{c1}, is signaled when the initial M-versus-H_{int} curve deviates from linearity, indicating flux penetration and the "mixed" state. (The intermediate state is also possible in type-II superconductors.)

HYSTERESIS LOSS

We now consider hysteresis loss in superconductors. Theoretical loss expressions are usually given in terms of the applied field, H_{ext}. While a hysteresis loop plotted as M versus H_{int} is generally shaped differently from one plotted as M versus H_{ext}, the areas enclosed by the loops are the same. This can be seen by integrating H_{int} as a function of M and referring to Eq. 1, as we now show.

Consider a hysteresis loop plotted as M versus H_{int}. Let the end points of the loop be denoted as 1 and 2. The two points are joined by curves A and B. Using the usual convention of integrating H as a function of M, the area of the loop enclosed by curves A and B is

$$W = \int_1^2 H_{int}^A \, dM - \int_1^2 H_{int}^B \, dM \tag{5}$$

$$= \int_1^2 H_{ext}^A \, dM - D \int_1^2 M \, dM - \int_1^2 H_{ext}^B \, dM + D \int_1^2 M \, dM$$

$$= \int_1^2 H_{ext}^A \, dM - \int_1^2 H_{ext}^B \, dM \, . \tag{6}$$

Thus, the loop areas are the same for both M versus H_{int} and M versus H_{ext}.

MULTIFILAMENTARY SUPERCONDUCTORS

The fields in the somewhat special case of a multifilamentary superconductor have been analyzed by Carr [2-4]. In the equations, M now refers to the magnetic moment per unit volume of superconductor, not including matrix material. Often, however, M is expressed as magnetic moment per total

volume and the volume fraction of superconductor is carried in the equations. For hysteresis calculations, the local field, H_{loc}, applied to each filament is used rather than H_{ext} applied to the composite conductor. H_{loc} is sometimes referred to as the Lorentz or cavity field:

$$H_{loc} \equiv H_{int} + DM \ . \tag{7}$$

For H_{ext} applied axially to the conductor (and filaments), $H_{loc} = H_{ext} = H_{int}$.

For H_{ext} applied transversely, $H_{loc} = H_{int} + M/2$. For the special case when H_{ext} is changed slowly and there is no transport current, Eq. 1 applies: $H_{int} = H_{ext} - M/2$. Thus, $H_{loc} = H_{ext}$. Therefore, we can continue to use H_{ext} in the hysteresis loss calculations for this special case. Similarly, χ_{loc}, equal to dM/dH_{loc} for multifilamentary conductors, will equal χ_{ext}. For the general transverse case, however, shielding effects prevent us from using H_{loc} and H_{ext} interchangeably.

We summarize the equations for χ_{int} and χ_{ext} when there is no shielding and the volume fraction of superconductor, λ, is carried in the equations [2,4]. We have, for H_{ext} applied axially,

$$\chi_{int} = \chi_{ext} = -\lambda \ . \tag{8}$$

The expressions for H_{ext} applied transversely are

$$\chi_{int} = -2\lambda/(1+\lambda) \ , \tag{9}$$

$$\chi_{ext} = -2\lambda \ . \tag{10}$$

Equations 9 and 10 are related by Eqs. 2 and 3.

EFFECTIVE DEMAGNETIZATION FACTOR FOR COILS

Sumiyoshi et al. derived an effective demagnetization factor, D_{eff}, for a single-layer coil of multifilamentary superconductor parallel to the coil axis [5]. That is, H_{ext} is applied transversely to the conductor.

$$D_{eff} = [1 - \cos(\pi r/d)] \ / \ [\cosh(\pi r/d) - \cos(\pi r/d)] \tag{11}$$

Here, r is the radius of the filament bundle and 2d is the center-to-center separation of the bundles. D_{eff} takes into account the interaction between the turns of the coil. We assume that there is no current in the conductor.

In the limiting case where d >> r, $D_{eff} = 1/2$, as for isolated transverse cylinders. In the other limit, d = r, $D_{eff} = 0.1588$. Thus from Eq. 4, χ_{ext} can range from -2 to -1.189.

The effect of coil-turn interaction has also been discussed by Carr et al. [6], Zenkevitch and Romanyuk [7], and Campbell [8].

CONCLUSION

The correct analysis of magnetization data requires that one account for demagnetization factors and internal fields. This applies to magnetic materials as well as superconductors.

ACKNOWLEDGMENT

This work was sponsored by the Air Force Office of Scientific Research.

REFERENCES

1. E. A. Lynton, "Superconductivity," Methuen, London (1962) p. 25.

2. W. J. Carr, Jr., Electromagnetic theory for filamentary superconductors, Phys. Rev. B 11, 1547 (1975).

3. W. J. Carr, Jr., "AC Loss and Macroscopic Theory of Superconductors," Gordon and Breach (1983) pp. 97-101.

4. W. J. Carr, Jr. and G. R. Wagner, Hysteresis in a fine filament NbTi composite, in: "Advances in Cryogenic Engineering (Materials)," Vol. 30, A. F. Clark and R. P. Reed, eds. (1984) pp. 923-30.

5. F. Sumiyoshi, F. Irie, and K. Yoshida, The effect of demagnetization on the eddy-current loss in a single-layered multifilamentary superconducting coil, J. Appl. Phys. 51, 3807 (1980).

6. W. J. Carr, Jr., B Clawson, and W. Vogen, AC losses in superconducting solenoids, IEEE Trans. Magn. MAG-14, 617 (1978).

7. V. B. Zenkevitch and A. S. Romanyuk, Effect of magnetic properties of a composite superconductor on the losses in a variable magnetic field. Part 3: Collective interaction of turns, Cryogenics 20, 79 (1980).

8. A. M. Campbell, A general treatment of losses in multifilamentary superconductors, Cryogenics 22, 3 (1982).

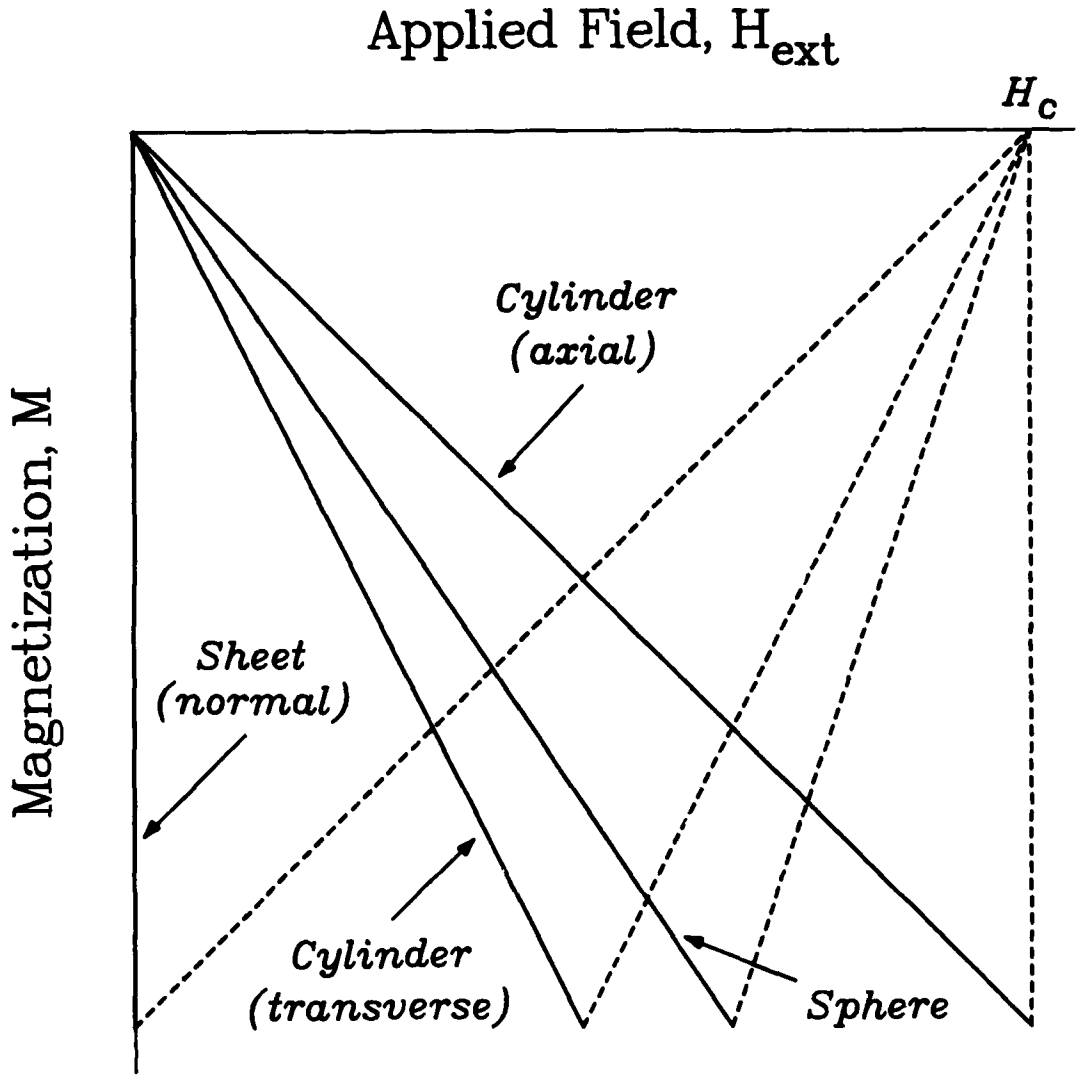

Figure 1. Magnetization versus external applied field for an ideal type-I superconductor of various geometries. The external susceptibilities are given by the initial slopes. The broken lines indicate flux penetration for the intermediate states. After Lynton [1].

Calibration of ac susceptometer for cylindrical specimens

R. B. Goldfarb and J. V. Minervini

Electromagnetic Technology Division, National Bureau of Standards, Boulder, Colorado 80303

(Received 11 November 1983; accepted for publication 30 January 1984)

The absolute magnetic susceptibility of cylindrical specimens is obtained with an ac susceptometer whose calibration is based on a calculation of mutual inductance. An axially magnetized cylinder is modeled as a solenoid of the same size. The mutual inductance between such a solenoid and a pickup coil of arbitrary dimensions is computed. The susceptibility is then a function of the mutual inductance, the cylinder length, the magnitude and frequency of the ac magnetizing field, and the voltage induced on the pickup coil. Demagnetization factor and eddy-current effects are considered, an example is given, and pickup coil compensation is discussed. Other calibration methods are also presented.

PACS numbers: 07.55. + x

INTRODUCTION

A useful method of measuring the magnetic susceptibility of nonferromagnetic materials employs an ac field source and a pickup coil. A typical circuit is shown in Fig. 1. Such pickup coils usually require calibration with standards of similar size to that of the specimens under study, except for the case of thin pickup coils with ellipsoidal samples, whose dipolar fields allow a closed-form mathematical solution.[1]

A method of calibration of an ac susceptometer for relatively long cylindrical specimens of arbitrary dimensions, coaxial with a pickup coil, is based on a calculation of mutual inductance. The mutual inductance between two coaxial coils (inner and outer) may be numerically computed. Since the flux density distribution of a uniformly, longitudinally magnetized cylinder of uniform composition is the same as that of a solenoid of the same size, a cylindrical specimen may be modeled as an inner coil. The calculation of mutual inductance leads to the absolute magnetic volume susceptibility of the cylinder, when an ac field is applied, in terms of the emf induced on the outer pickup coil.

I. CALIBRATION BY CALCULATION OF MUTUAL INDUCTANCE

A. Equivalent solenoid

In general, the flux density **B** may be thought of as due to Amperian currents of volume density $\nabla\times\mathbf{M}$ and surface density $\mathbf{M}\times\hat{n}$, where **M** is the magnetization and $\hat{n}$ is the unit vector normal to the surface. The flux density **B** external to a cylinder of uniform axial magnetization ($\nabla\times\mathbf{M}=0$) is equivalent to that of a model solenoid of the same size with ampere-turn density NI/l, where M has units A/m, N is the number of turns, I is the current, and l is the length:

$$M = NI/l. \tag{1}$$

The near field cannot be expressed in closed form, but may be computed by superposition of **B** due to elemental uniformly magnetized disks or elemental circular current loops for the cylinder or equivalent solenoid, respectively. The near field of a current loop is well known.[2,3]

The total magnetic flux (flux linkage) Φ sensed by the pickup coil may be calculated from either **B** or the vector potential **A**:

$$\Phi = \iint \mathbf{B}\cdot d\mathbf{a} = \oint \mathbf{A}\cdot d\mathbf{s}, \tag{2}$$

where $d\mathbf{a}$ is the incremental area, $d\mathbf{s}$ is the incremental contour, and the integrations are over the entire pickup coil. The mutual inductance per solenoid turn is

$$L^* = L_{12}/N = \Phi/NI = \frac{1}{NI}\oint \mathbf{A}\cdot d\mathbf{s}, \tag{3}$$

where L_{12} is the mutual inductance between the solenoid and the pickup coil. L_{12} is proportional to N; L^* is independent of N but depends on the geometries of the solenoid (i.e., specimen) and the pickup coil, and the number of turns on the pickup coil. A general mutual inductance calculation is detailed in Sec. I B. The emf induced in the pickup coil due to the solenoid is

$$v = -d\Phi/dt = -L_{12}\,dI/dt. \tag{4}$$

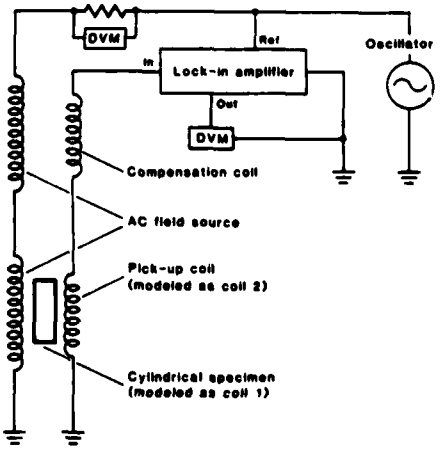

FIG. 1. One method [see number (6) in Table II] of measuring ac susceptibility.

Converting current to magnetization using Eq. 1,

$$v = -L^* l\, dM/dt. \tag{5}$$

To this point, the ac field source has not been part of the derivation. In fact, *it has been and will continue to be assumed that the emf induced in the pickup coil by the field source is nulled* (see Sec. II B). The ac field is assumed to be uniform. Substituting $M = \chi H$, where χ is the volume susceptibility (dimensionless), $H = H_0 \cos 2\pi ft$ is the applied ac magnetic field, and rearranging Eq. (5), the final result is obtained:

$$\chi = \frac{v_{\rm rms}}{L^* l\, 2\pi f H_{\rm rms}}, \tag{6}$$

where f is in hertz and χ is in SI units. To convert to cgs units, the value of χ is divided by 4π. The assumption of uniform M and H is a good one for relatively long cylinders characterized by small demagnetiztion factors (see Sec. I C).

B. Mutual inductance of coaxial solenoids

The mutual inductance [L_{12} in Eq. (3)] may be calculated using computer techniques for the general case of coaxial, but not necessarily concentric, thick solenoids. Figure 2 shows the geometry and defines some of the variables. The mutual inductance is calculated by integrating A, due to a current density J in coil 1, around the turns of coil 2. The vector potential A has only a ϕ component. At the point (r,ϕ,z) in cylindrical coordinates,[4]

$$\mathbf{A}_\phi(r,z) = \frac{\mu_0 J}{4\pi}\int_{a_{11}}^{a_{12}} da\, a \int_0^{2\pi} d\theta \cos\theta \ln[\xi + (\xi^2 + r^2 + a^2 - 2ar\cos\theta)^{1/2}]\Big|_{\xi_1}^{\xi_2}$$
$$= \frac{\mu_0 J}{4\pi}\int_{a_{11}}^{a_{12}} da\, a^2 \int_0^{2\pi} d\theta \left(\frac{\xi r \sin^2\theta}{(a^2 + r^2 - 2ar\cos\theta)(\xi^2 + r^2 + a^2 - 2ar\cos\theta)^{1/2}}\right)_{\xi_1}^{\xi_2} \equiv \frac{\mu_0 J}{4\pi}\Lambda(r,z), \tag{7}$$

where $\xi = z - \lambda$, $\xi_1 = z - l/2$, $\xi_2 = z + l/2$, and the cylindrical coordinates of each current element are a, θ, λ. J is assumed constant and is simply

$$J = \frac{NI}{l(a_{12} - a_{11})}. \tag{8}$$

From the expression for L_{12} in Eq. (3), and using Eqs. (7) and (8)

$$L_{12} = \frac{\mu_0 N}{4\pi l (a_{12} - a_{11})}\oint \Lambda(r,z)\cdot ds, \tag{9}$$

where I is canceled. For the purpose at hand, $a_{12} \gtrsim a_{11} = d/2$, where d is the specimen diameter. All that remains is to compute the contour integral of Λ.

For purposes of computation, coil 2 is divided into $n \times m$ circular rings, usually not coincident with the actual windings (see Fig. 2). The radius of each ring is

$$r_i = a_{21} + (i - \tfrac{1}{2})(a_{22} - a_{21})/n, \quad i = 1,2,\ldots,n, \tag{10}$$

and its position is

$$z_j = z_d - \tfrac{1}{2}l_2 + (j - \tfrac{1}{2})l_2/m, \quad j = 1,2,\ldots,m. \tag{11}$$

The double integral Λ [given in Eq. (7)] is evaluated for each ring located at (r_i, z_j) using a standard library routine. Then the contour integral of Λ in Eq. (9) is simply

$$\oint \Lambda(r,z)\cdot ds = \frac{N_2}{mn}\sum_{i=1}^{n}\sum_{j=1}^{m} 2\pi r_i\, \Lambda(r_i, z_j), \tag{12}$$

where ds is $r\, d\phi$. The factor N_2/mn is introduced to scale L_{12} to reflect the actual number of turns in coil 2. If the coil displacement z_d is zero (the usual case when the specimen cylinder is centered in the pickup coil), the index j can run from 1 to $m/2$ and the result for L_{12} doubled, thereby taking advantage of the axial symmetry. The number of $n \times m$ discrete segments should be chosen to optimize the tradeoff between accuracy and computation time.

Other procedures may be used to calculate L_{12}. Thin-coil approximations are clearly suitable for the model solenoid and are often adequate for the pickup coil.[5]

C. Demagnetization factor considerations

When susceptibilities are large or when cylinders are not too long, the measured χ should be corrected for demagnetization fields

$$\chi_{\rm int} = \chi/(1 - D\chi), \tag{13}$$

where $\chi_{\rm int}$ is the "internal" susceptibility, corrected for demagnetization, and D is the demagnetization factor ($0 < D < 1$ in SI). Exact values of D are obtainable only for ellipsoids. Average values for uniformly magnetized cylinders have been computed by Brown[6,7] and Crabtree[8] and are given in Table I. These "magnetometric" values are greater than those "ballistic" values reported by Bozorth and Chapin[9] for highly permeable rods. The latter were experimentally determined and based on the magnetization at the middle of a rod rather than an average over the entire volume. Note that the approximation of uniform longitudinal mag-

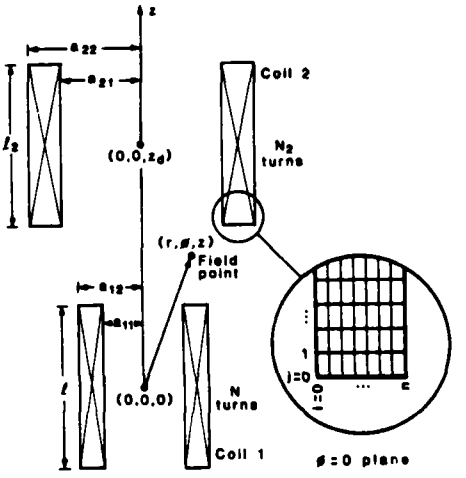

FIG. 2. Geometry for mutual inductance calculations.

netization is realistic only in the cases of materials with small susceptibilities, or relatively long cylinders characterized by small demagnetization factors. Therefore, calculations with cylinders are always approximate to some degree.

D. Eddy current considerations

The eddy currents induced in a conducting material exposed to an alternating magnetic field are a function of the material's susceptibility, resistivity, and geometry. These currents give rise to an internal field which differs from the applied field in magnitude and phase. For accurate susceptibility measurements, these deviations should be minimized.

Zijlstra[10] examines the case of an infinitely long cylinder subject to an ac axial field. The deviations in field magnitude and phase are a function of the reduced radius

$$a_0 = d/\sqrt{2}\delta, \tag{14}$$

where d is the cylinder diameter and δ is the skin depth,

$$\delta = (\rho/\pi f\mu)^{1/2}, \tag{15}$$

where ρ is the material resistivity, f is the frequency, and μ is the permeability equal to $\mu_0(1+\chi)$, where μ_0 is the permeability of free space.

The analysis shows that magnitude errors in χ are less than 3% when $a_0 < 0.9$ and that errors in both magnitude and phase are negligible when $a_0 < 0.2$. The restriction on a_0 may be met by reducing d and f, since ρ and μ are materials properties.

II. EXPERIMENT

A. Example

The dependence of L^* upon a cylinder's length and diameter was computed for a specific pickup coil for illustrative purposes. A plot is shown in Fig. 3. The normalization of the variables applies to this particular coil only.

The room temperature susceptibility of a sample of AISI-type 316 stainless steel was measured using this coil.

TABLE I. Longitudinal demagnetization factors D for cylinders as a function of the ratio of length to diameter l/d [after Crabtree (Ref. 8)].

l/d	D	l/d	D	l/d	D
0.0	1.000	2.0	0.181	4.0	0.0978
0.1	0.796	2.1	0.174	4.1	0.0956
0.2	0.680	2.2	0.167	4.2	0.0935
0.3	0.594	2.3	0.161	4.3	0.0914
0.4	0.528	2.4	0.155	4.4	0.0895
0.5	0.474	2.5	0.149	4.5	0.0876
0.6	0.430	2.6	0.144	4.6	0.0858
0.7	0.393	2.7	0.140	4.7	0.0841
0.8	0.361	2.8	0.135	4.8	0.0824
0.9	0.334	2.9	0.131	4.9	0.0808
1.0	0.311	3.0	0.127	5.0	0.0793
1.1	0.291	3.1	0.123	5.5	0.0723
1.2	0.273	3.2	0.120	6.0	0.0666
1.3	0.257	3.3	0.116	6.5	0.0616
1.4	0.242	3.4	0.113	7.0	0.0573
1.5	0.230	3.5	0.110	7.5	0.0536
1.6	0.218	3.6	0.107	8.0	0.0503
1.7	0.207	3.7	0.105	8.5	0.0473
1.8	0.198	3.8	0.102	9.0	0.0447
1.9	0.189	3.9	0.100	10.0	0.0403

The result was verified with a SQUID susceptometer. A cylinder of length 10.2 cm and diameter 1.2 cm was prepared. L^* was computed to be 14 μH for the combination of cylinder and pickup coil. An ac field of 570-A/m rms at 100 Hz was applied. χ was found to be 2.9×10^{-3} (SI). This approximates the smallest values of susceptibility which can be accurately measured with the present apparatus. A small piece of steel was obtained from the same rod stock for SQUID measurement. Using a density of 7.958 g/cm^3,[11] χ was 3.0×10^{-3}, in good agreement with the mutual inductance method. Taking a resistivity of 75 $\mu\Omega$ cm,[12] and applying the eddy-current criterion of Sec. I D, a_0 is found to be 0.195, which is very acceptable.

B. Coil compensation

As mentioned in Sec. II A, the background emf of the pickup coil with no sample present needs to be subtracted from the measured emf with the sample in place. This may be done by the various methods shown in Table II. Methods (4), (5), and (6) seem to be satisfactory; method (6), illustrated in Fig. 1, is the least expensive and most straightforward.

III. OTHER CALIBRATION METHODS

A. Change in self-inductance

A variation of the method described in Sec. I A is that of relating the change in self-inductance of a pickup coil, after a specimen is inserted, to the magnetic susceptibility of the specimen. This technique may be used with a commercial inductance meter equipped with a convenient zero offset. Such devices may be thought of as applying a sinusoidal current to a test coil and measuring the voltage across it. The following equations apply:

$$v_s = -L_s \frac{dI}{dt}, \tag{16}$$

where L_s is the self-inductance,

$$I = I_0 \cos 2\pi ft, \tag{17}$$

$$v_{s,\mathrm{rms}} = 2\pi f I_{\mathrm{rms}} L_s. \tag{18}$$

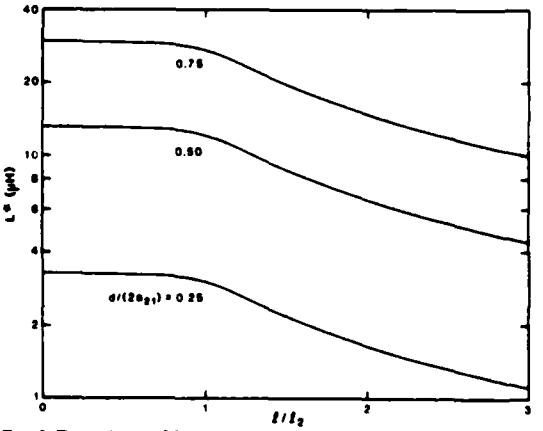

FIG. 3. Dependence of L^* upon cylinder length and diameter. The pickup coil parameters are: $a_{21} = 11.9$ mm, $a_{22} = 13.3$ mm, $l_2 = 127$ mm, $N_2 = 6042$, $z_d = 0$.

Erratum: Page 763, second column, line 3 and Fig. 3: "L*" should be "2L*"

TABLE II. Various methods of pickup coil compensation.

	Method of coil compensation	Remarks
(1)	Subtract dc output of lock-in amplifier for empty pickup coil	Simple; poor resolution because $\Delta v/v$ is small
(2)	Null dc output of lock-in amplifier using internal offset	Simple; offset works only over limited range
(3)	Subtract ac signal of pickup coil using digital recording oscilloscope	Any phase shift caused by eddy currents gives errors
(4)	Subtract rms level of ac signal of pickup coil using digital oscilloscope	Digital processing and noise filtering needed
(5)	Subtract an ac waveform equal to that of empty pickup coil, using a differential amplifier, before input to lock-in amplifier	Need stable phase-lock phase shifter with variable gain; eddy-current phase shifts give errors
(6)	Series matched, counterwound "bucking" coil to null sample pickup coil	Both coils must be exposed to same ac field

From Eq. (6), the sample contribution to the voltage is

$$v_{\rm rms} = L^{*}l\chi 2\pi f H_{\rm rms}. \tag{19}$$

The field $H_{\rm rms}$ is proportional to the current in the coil

$$H_{\rm rms} = cI_{\rm rms}, \tag{20}$$

where c is a constant of dimension m^{-1}. The total voltage is

$$v_{s,\rm rms} + v_{\rm rms} = 2\pi f I_{\rm rms}(L_s + cL^{*}l\chi)$$
$$\equiv 2\pi f I_{\rm rms}(L_s + \Delta L). \tag{21}$$

The volume susceptibility is obtained from the increase in inductance ΔL when the specimen is inserted in the coil

$$\chi = \frac{\Delta L}{cL^{*}l}. \tag{22}$$

This method, relying on the coil for both field and pickup, is less sensitive than the method in Sec. I A.

B. Calibration with standards

It is often desirable to calibrate susceptometers experimentally, which requires the use of standards. The resulting calibration is strictly valid only for specimens of the same size and shape as the standard used.

1. Materials with known susceptibility

The NBS Office of Standard Reference Materials sells four susceptibility standards: Al, Pt, Pd, and MnF_2, with χ ranging from 2×10^{-5} to 6×10^{-3} (SI) at room temperature.[13] They are available in various forms.

2. Soft ferromagnets with "infinite" internal susceptibility and known demagnetization factor

An example is a spherical sample of Gd near its Curie temperature. Some provision for cooling is needed to experimentally obtain the maximum pickup voltage.

The susceptibility χ is generally proportional to the pickup coil voltage v, and inversely proportional to the sample volume V, the ac field H, and its frequency f:

$$\chi = av/Vf H. \tag{23}$$

The empirical calibration constant a is obtained by measuring the pickup coil voltage v_0 for a sphere of volume V_0 and demagnetization factor 1/3 in a field H_0 of frequency f_0. Assuming an infinite $\chi_{\rm int}$, Eq. (13) yields

$$1 - D\chi_0 = 0, \tag{24}$$

whence the measured susceptibility $\chi_0 = 3$. Thus,

$$a = 3V_0 f_0 H_0/v_0. \tag{25}$$

3. Superconducting materials with known demagnetization factor

An example is a spherical sample of Nb below its critical temperature. The ability to cool to cryogenic temperatures is required. The perfect diamagnetism ($\chi_{\rm int} = -1$) of superconductors arises from the Meissner effect. From Eq. (13),

$$\chi_0 = D\chi_0 - 1, \tag{26}$$

and for the sphere, $\chi_0 = -3/2$, or 3/2 but 180° out of phase. Equation (23) applies with

$$a = 3V_0 f_0 H_0/2v_0. \tag{27}$$

Similar calibrations may be done, of course, with cylindrical standards using the approximate demagnetization factors in Table I. Methods of preparing spheres are described in Ref. 14.

ACKNOWLEDGMENTS

F. R. Fickett, S. M. Goodnick, C. A. Hamilton, and D. A. Krueger commented critically and valuably on the manuscript. The work was partially funded by the Air Force Office of Scientific Research.

[1] See, for example, the result given in W. R. Abel, A. C. Anderson, and J. C. Wheatley, Rev. Sci. Instrum. 35, 444 (1964).
[2] J. D. Jackson, *Classical Electrodynamics* (Wiley, New York, 1962), pp. 142 and 143.
[3] W. R. Smythe, *Static and Dynamic Electricity*, 3rd ed. (McGraw-Hill, New York, 1968), pp. 290 and 291.
[4] The derivation of the vector potential for a thick solenoid may be found in G. V. Brown, L. Flax, E. C. Itean, and J. C. Laurence, NASA Tech. Report No. TR R-170, December 1963, available at NTIS, Springfield, Virginia, N64-15331.
[5] Formulas and tables for the mutual inductance of coaxial, single-layer coils may be found in F. W. Grover, *Inductance Calculations* (Van Nostrand, New York, 1946), Chap. 15; E. B. Rosa and F. W. Grover, Bull. Bur. Stand. 8, 1 (1912).
[6] W. F. Brown, Jr., Am. J. Phys. 28, 542 (1960).
[7] W. F. Brown, Jr., *Magnetostatic Principles in Ferromagnetism* (North-Holland, Amsterdam, 1962), pp. 187–192. The magnetometric demagnetization factors may be obtained from the *self*-inductance of the model solenoid.
[8] G. W. Crabtree, Phys. Rev. B 16, 1117 (1977).
[9] R. M. Bozorth and D. M. Chapin J. Appl. Phys. 13, 320 (1942).
[10] H. Zijlstra, *Experimental Methods in Magnetism* (North-Holland, Amsterdam, 1967), Vol. 2, pp. 72–79.
[11] H. M. Ledbetter, Met. Sci. 14, 595 (1980).
[12] F. R. Fickett, in *Materials at Low Temperatures*, edited by R. P. Reed and A. F. Clark (American Society for Metals, Metals Park, Ohio, 1983), Chap. 5, p. 197.
[13] NBS Spec. Publ. 260 (Office of Standard Reference Materials, National Bureau of Standards, Washington, D. C., 1981).
[14] J. N. Paranto and C. E. Patton, Rev. Sci. Instrum. 52, 262 (1981).

QUENCH CIRCUIT FOR ELECTRONIC INSTRUMENTS USED WITH SUPERCONDUCTING MAGNETS

R. G. Benson, R. B. Goldfarb, and E. S. Pittman
Electromagnetic Technology Division
National Bureau of Standards
Boulder, Colorado 80303

ABSTRACT

A multifunction circuit is described that protects, in the event of a quench, instruments connected or coupled to a superconducting magnet.

INTRODUCTION

Most laboratory superconducting magnets are suitably protected against damage if they revert to the normal state (quench). Often it is desirable to provide protection for instruments connected or coupled to such a magnet. Such protection is provided by a circuit that performs three functions: (1) sends an interrupt command to a computer via an interface card, (2) protects an analog-to-digital (A/D) card that monitors the magnet voltage from large voltages generated during a quench, and (3) shorts the output of a digital-to-analog (D/A) programming-voltage card and thus nulls the output of the magnet current supply. A diode bank that protects a magnet power supply is also described.

QUENCH DETECTION CIRCUIT

A superconducting magnet in our laboratory is powered by a constant-current supply. This power supply, programmed with the dc voltage output of a D/A card, is bipolar and referenced to ground. The D/A card is controlled by a microcomputer. The magnet voltage, L dI/dt, is sensed by an A/D card which

in turn is connected to the computer. By monitoring this voltage, the computer is able to determine when the magnet has finished charging or discharging.

In the event of a quench, we wish to: (1) inform the computer that a quench has occurred by enabling the interrupt card, (2) protect the A/D card against possible high magnet voltages, and (3) bring the power supply output to zero by nulling the programming voltage of the current supply.

We designed and constructed a circuit to perform these tasks. The input is connected across the magnet. The circuit's input impedance is greater than 500 kΩ. A comparator-threshold adjustment sets the voltage criterion for a quench (e.g., 3.5 V). A time-constant adjustment prevents the quench detector from triggering on random, transient voltage spikes. This sets a time delay of, typically, 10 to 250 ms for actual quench detection. When a quench is detected, an LED turns on. Once the magnet voltage has decreased to below the quench-detection threshold, pressing the RESET button rearms the circuit.

The circuit schematic is shown in Fig. 1. There are three outputs: INTERRUPT, A/D OUT, and D/A OUT. (1) When a quench is detected, a logical "1" is sent to the interrupt card. (2) A/D OUT normally sends the magnet voltage to the A/D card. In the event of a quench, a relay breaks this connection. Additional protection is provided by a series fuse. Finally, two Zener diodes, D3, in parallel with the output prevent the magnitude of the output voltage from exceeding 12 V. (3) D/A OUT is normally an open switch in parallel with the output of the D/A card. When a quench occurs, Relay A closes, forcing the programming voltage of the magnet current supply to zero. (The D/A card is internally current limited.)

The circuit is divided into several stages: input protect, absolute value, voltage comparator, latch logic, and output stages.

Input protect. Large voltage spikes dissipate power in resistor R1. The input voltage to the rest of the circuit is limited to about 10 V by the two Zener diodes D1.

Absolute value. The absolute value stage uses two operational amplifiers, A1 and A2, and has a positive output with unity gain. For positive input voltages, diode D2 is reverse biased, A2 is effectively removed from the circuit, and A1 is a unity-gain amplifier. For negative voltages, D2 is forward biased, the positive input to A1 is grounded, and A1 acts as an inverter.

Voltage comparator. The comparator produces a low output of zero volts for inputs greater than the reference voltage and a high output of 4 V otherwise. The feedback resistor provides some hysteresis in the comparator. The QUENCH-THRESHOLD adjustment R2 sets the comparator reference voltage V_{ref}. The TIME-CONSTANT adjustment R3 is part of a simple RC filter.

Latch logic. When the circuit is turned on, the 10-μF capacitor C1 holds the CLEAR input to ground long enough to allow the flip-flop to start in the cleared state (Q low and $\bar{Q}$ high). After about 10 ms, the CLEAR input goes high. It can be set low with the RESET button. When a quench is detected, the output of the voltage comparator goes low and SET becomes active, causing Q to go high and $\bar{Q}$ low.

Output stages. When Q is high, a logical "1" is sent to the interrupt card. Also, transistor T1 is turned on, which lights the LED and closes Relay A. This in turn shorts D/A OUT, which zeros the programming voltage to the power supply. When $\bar{Q}$ is low, transistor T2 is turned off. This opens Relay B, which protects the A/D card.

POWER SUPPLY PROTECTION

Power supplies designed for use with superconducting magnets are often built with quench protection. A quench is accompanied by large voltages (typically a few hundred volts) and currents of polarity opposite that of the charge current. Most power supplies are not designed to sink reverse current. In the case of a unipolar dc supply, adequate protection may be provided by a reverse-biased, heat-sinked power diode across the output terminals, in parallel with the magnet leads.

In the case of a bipolar supply, however, the forward voltage drop of the diode would be too small for negative-current operation; magnet charging voltages are often as great as 3 V. We have constructed an array of heat-sinked 1N3111 diodes to protect such bipolar supplies. The circuit is shown in Fig. 2. It is connected across the output of the power supply, in parallel with the magnet leads. The diode array does not conduct for typical magnet charging voltages. If quench voltages are large in either polarity, the array conducts, thereby protecting the power supply. The six diodes in series in either direction begin to conduct at 4 V and conduct well at 5 V.

ACKNOWLEDGEMENT

This work was sponsored by the Air Force Office of Scientific Research.

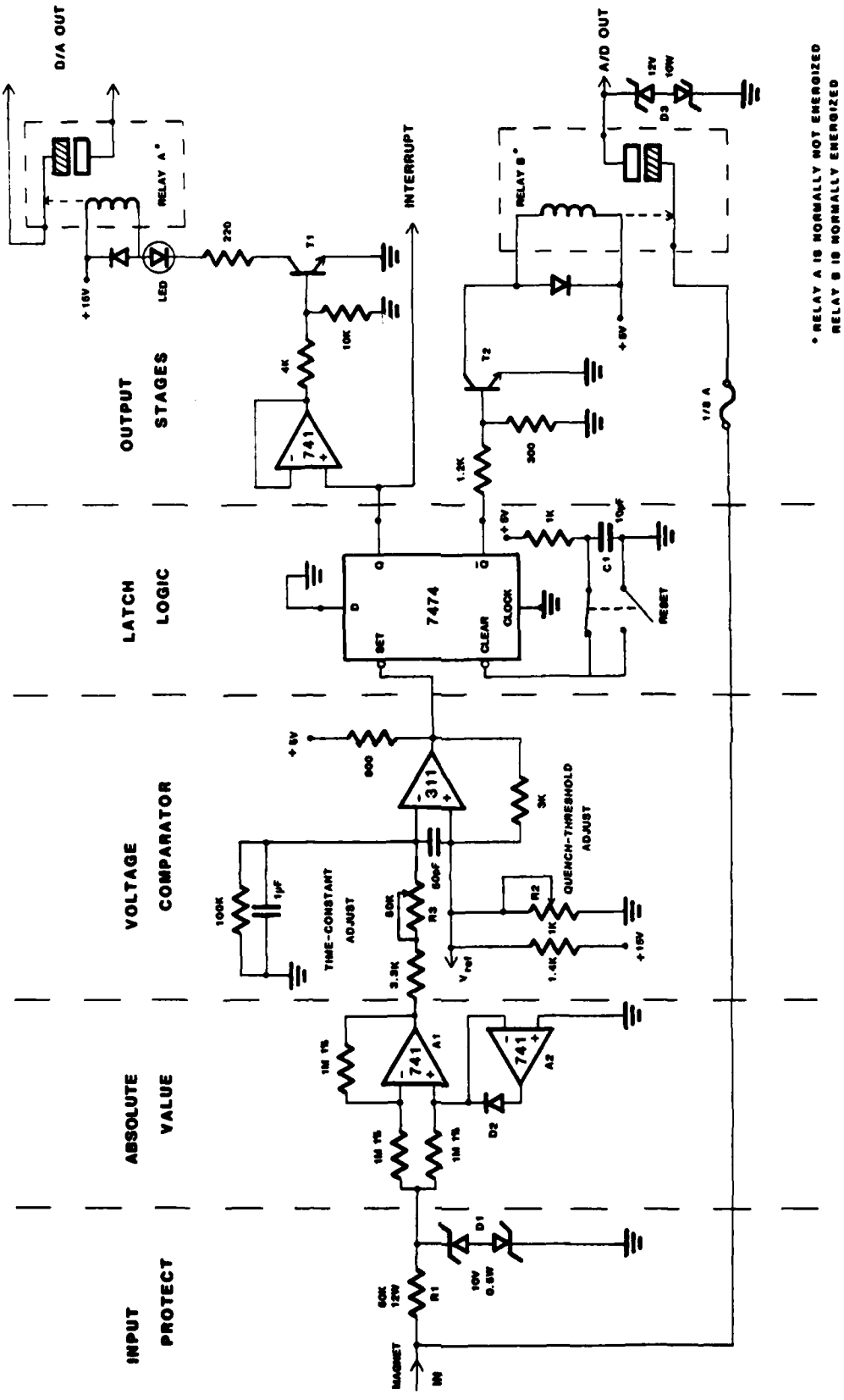

Figure 1. Quench protection circuit.

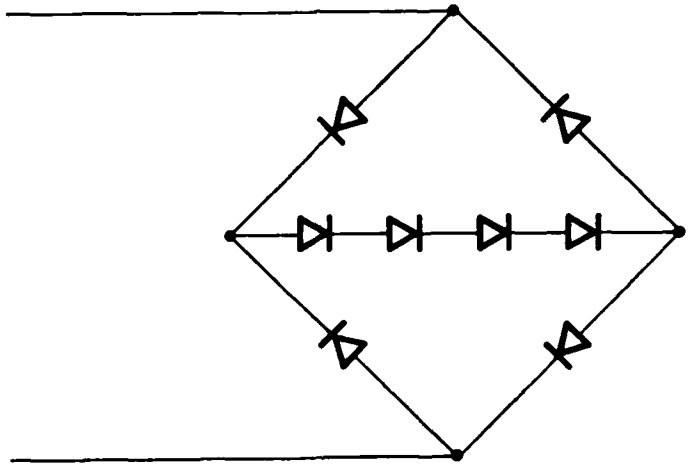

Figure 2. Diode array for power supply protection.

CHARACTERIZATION OF ALLOYS

R. B. Goldfarb
Electromagnetic Technology Division
National Bureau of Standards
Boulder, Colorado 80303

I. PHYSICAL CHARACTERISTICS OF MULTIFILAMENTARY Nb-Ti SUPERCONDUCTORS

We have found that, except for the number of Nb-Ti filaments, superconductor wire manufacturers often do not reliably report the physical characteristics of their wires. For accurate magnetization and loss calculations, however, we must know the copper-to-superconductor volume ratio and the filament radius in addition to measured magnetic moment. It is also useful to know the density of the Nb-Ti alloy. This note describes how we determine these parameters.

A 1.000-meter length of wire is stripped of its insulation. We measure its mass, m_{wire}. Using Archimedes' principle, we determine its volume, V_{wire}. The wire is then soaked in a 50% solution of nitric acid and water to remove the copper, leaving only the Nb-Ti filaments. The filaments are rinsed and thoroughly dried. We then measure their mass, m_{fil}. We do not directly determine the volume of the filaments, V_{fil}, because of the danger of trapping air bubbles upon immersion in water. Instead, we calculate the mass of copper, $m_{Cu} = m_{wire} - m_{fil}$, and use the known density of pure Cu (8.93 g/cm^3) to calculate the volume of copper, V_{Cu}. Then, $V_{fil} = V_{wire} - V_{Cu}$.

The copper-to-superconductor volume ratio is then V_{Cu}/V_{fil}. The density of the Nb-Ti alloy is m_{fil}/V_{fil}. The filament radius is $(V_{fil}/\pi NL)^{\frac{1}{2}}$, where N is the number of filaments given by the manufacturer and L is the length (1.000 m).

II. CONVERSION OF ATOMIC AND WEIGHT PERCENTS

Let the atomic masses of the elements be denoted by A_i, the atomic percents be denoted by a_i, and the weight percents be denoted by w_i. By definition, $\Sigma a_i = 1$ and $\Sigma w_i = 1$.

To convert atomic to weight percent:

$$w_i = a_i A_i / \Sigma a_j A_j \quad . \tag{1}$$

The average atomic mass of the alloy is $\bar{A}$:

$$\bar{A} \equiv \Sigma a_j A_j \quad . \tag{2}$$

Thus,

$$w_i = a_i A_i / \bar{A} \quad . \tag{3}$$

To convert weight to atomic percent:

$$a_i = (w_i/A_i)/\Sigma(w_j/A_j) \quad . \tag{4}$$

As pointed out by H. M. Ledbetter (private communication), substituting Eq. 4 into Eq. 2 gives

$$\bar{A} = [\Sigma(w_j/A_j)]^{-1} \quad . \tag{5}$$

Thus,

$$a_i = (w_i/A_i)\ \bar{A} \quad . \tag{6}$$

III. DENSITIES OF SUBSTITUTIONAL BINARY ALLOYS

Often we wish to deduce the density of a binary alloy by interpolation from the densities of the pure elements. There are two approaches. The first is to assume that both elements have the same atomic volumes. We then interpolate by substituting the atomic mass of one for the atomic mass of the other. The second approach is to assume the same atomic masses. We then interpolate by substituting the atomic volumes. Both methods are presented below, applied to the Nb-Ti system. In this example, where the atomic masses of Nb and Ti are known to be very different, the first approach is better.

Symbols

Subscripts indicate element 1 or 2

- ρ = density
- m = mass per atom
- v = volume per atom
- n = number of atoms per cm^3
- q = number of atoms per g
- a = atomic percent element 1
- w = weight percent element 1

Same Atomic Volumes

There is the same number of atoms per cm^3 for elements 1 and 2 ($n_1 = n_2$). The atomic mass of one is substituted for the atomic mass of the other.

$$\rho = nm \tag{7}$$

$$\rho_{alloy} = n[am_1 + (1-a)m_2]$$

$$= a\rho_1 + (1-a)\rho_2 \tag{8}$$

For example, $\rho_{Nb} = 8.57$ g/cm^3 and $\rho_{Ti} = 4.51$ g/cm^3. A "standard" alloy composition is 46.5 wt.% Ti = 63.0 at.% Ti. Thus,

$$\rho_{NbTi} = 6.012 \text{ g/cm}^3 \tag{9}$$

This compares favorably with a measured density of 6.004 g/cm^3.

Same Atomic Masses

There is the same number of atoms per g for elements 1 and 2 ($q_1 = q_2$). The atomic volume of one is substituted for the atomic volume of the other.

$$\rho^{-1} = qv \tag{10}$$

$$\rho_{alloy}^{-1} = q[uv_1 + (1-u)v_2]$$

$$= u/\rho_1 + (1-u)/\rho_2 \tag{11}$$

$$\rho_{alloy} = \rho_1\rho_2/[(\rho_1 + u(\rho_2-\rho_1)] \tag{12}$$

For the example of Nb-Ti of "standard" composition, we would obtain an inaccurate estimate: $\rho_{NbTi} = 5.784$ g/cm^3. The first method, assuming equal atomic volumes for the elements, is more suitable.

If the densities of certain alloy compositions are known, further refinement is possible by interpolating between them instead of the densities of the pure elements.

UNITS FOR MAGNETIC PROPERTIES

Quantity	Symbol	Gaussian & cgs emu [a]	Conversion factor, C [b]	SI & rationalized mks [c]
Magnetic flux density, magnetic induction	B	gauss (G) [d]	10^{-4}	tesla (T), Wb/m^2
Magnetic flux	Φ	maxwell (Mx), $G \cdot cm^2$	10^{-8}	weber (Wb), volt second (V·s)
Magnetic potential difference, magnetomotive force	U, F	gilbert (Gb)	$10/4\pi$	ampere (A)
Magnetic field strength, magnetizing force	H	oersted (Oe), [e] Gb/cm	$10^3/4\pi$	A/m [f]
(Volume) magnetization [g]	M	emu/cm^3 [h]	10^3	A/m
(Volume) magnetization	$4\pi M$	G	$10^3/4\pi$	A/m
Magnetic polarization, intensity of magnetization	J, I	emu/cm^3	$4\pi \times 10^{-4}$	T, Wb/m^2 [i]
(Mass) magnetization	σ, M	emu/g	1 $4\pi \times 10^{-7}$	$A \cdot m^2/kg$ Wb·m/kg
Magnetic moment	m	emu, erg/G	10^{-3}	$A \cdot m^2$, joule per tesla (J/T)
Magnetic dipole moment	j	emu, erg/G	$4\pi \times 10^{-10}$	Wb·m [i]
(Volume) susceptibility	χ, κ	dimensionless, emu/cm^3	4π $(4\pi)^2 \times 10^{-7}$	dimensionless henry per meter (H/m), Wb/(A·m)
(Mass) susceptibility	χ_ρ, κ_ρ	cm^3/g, emu/g	$4\pi \times 10^{-3}$ $(4\pi)^2 \times 10^{-10}$	m^3/kg $H \cdot m^2/kg$
(Molar) susceptibility	χ_{mol}, κ_{mol}	cm^3/mol, emu/mol	$4\pi \times 10^{-6}$ $(4\pi)^2 \times 10^{-13}$	m^3/mol $H \cdot m^2/mol$
Permeability	μ	dimensionless	$4\pi \times 10^{-7}$	H/m, Wb/(A·m)
Relative permeability [j]	μ_r	not defined		dimensionless
(Volume) energy density, energy product [k]	W	erg/cm^3	10^{-1}	J/m^3
Demagnetization factor	D, N	dimensionless	$1/4\pi$	dimensionless

a. Gaussian units and cgs emu are the same for magnetic properties. The defining relation is $B = H + 4\pi M$.

b. Multiply a number in Gaussian units by C to convert it to SI (e.g., $1\ G \times 10^{-4}\ T/G = 10^{-4}\ T$).

c. SI (*Système International d'Unités*) has been adopted by the National Bureau of Standards. Where two conversion factors are given, the upper one is recognized under, or consistent with, SI and is based on the definition $B = \mu_0(H + M)$, where $\mu_0 = 4\pi \times 10^{-7}$ H/m. The lower one is not recognized under SI and is based on the definition $B = \mu_0 H + J$, where the symbol I is often used in place of J.

d. 1 gauss = 10^5 gamma (γ).

e. Both oersted and gauss are expressed as $cm^{-1/2} \cdot g^{1/2} \cdot s^{-1}$ in terms of base units.

f. A/m was often expressed as "ampere-turn per meter" when used for magnetic field strength.

g. Magnetic moment per unit volume.

h. The designation "emu" is not a unit.

i. Recognized under SI, even though based on the definition $B = \mu_0 H + J$. See footnote *c*.

j. $\mu_r = \mu/\mu_0 = 1 + \chi$, all in SI. μ_r is equal to Gaussian μ.

k. $B \cdot H$ and $\mu_0 M \cdot H$ have SI units J/m^3; $M \cdot H$ and $B \cdot H/4\pi$ have Gaussian units erg/cm^3.

R. B. Goldfarb and F. R. Fickett, U.S. Department of Commerce, National Bureau of Standards, Boulder, Colorado 80303, March 1985
NBS Special Publication 696 For sale by the Superintendent of Documents, U.S. Government Printing Office, Washington, DC 20402

NBS-114A (REV. 2-8C)

U.S. DEPT. OF COMM. **BIBLIOGRAPHIC DATA SHEET** (See instructions)	1. PUBLICATION OR REPORT NO. NBSIR 86-3053	2. Performing Organ. Report No. AD-A1'	3. Publication Date June 1986

4. TITLE AND SUBTITLE

Transient Losses in Superconductors

5. AUTHOR(S)

R. B. Goldfarb, Editor

6. PERFORMING ORGANIZATION (If joint or other than NBS, see instructions)

NATIONAL BUREAU OF STANDARDS
DEPARTMENT OF COMMERCE
WASHINGTON, D.C. 20234

7. Contract/Grant No.

8. Type of Report & Period Covered
Final Report
1 Oct 1982 - 30 Sep 1985

9. SPONSORING ORGANIZATION NAME AND COMPLETE ADDRESS (Street, City, State, ZIP)

Air Force Office of Scientific Research
Bolling Air Force Base
Washington, DC 20332

10. SUPPLEMENTARY NOTES

☐ Document describes a computer program; SF-185, FIPS Software Summary, is attached.

11. ABSTRACT (A 200-word or less factual summary of most significant information. If document includes a significant bibliography or literature survey, mention it here)

Under steady-state conditions, there are no losses in superconducting wires. However, when subjected to alternating or transient magnetic fields or transport currents, losses in type-II superconductors can become significant. This report deals with hysteresis losses at 4 K measured by magnetization and complex magnetic susceptibility. The theoretical and experimental relationships between ac susceptibility and magnetization as functions of dc field were examined in terms of the critical-state model as developed by Carr and Clem. Minor-loop hysteresis loss was shown to be obtainable by direct measurement of loop area, from the imaginary component of ac susceptibility, and from the reversible susceptibility plus the critical current density or full-penetration field. Hysteresis and transport losses measured simultaneously in a Nb-Ti superconducting coil were found to agree substantially with the predictions of Minervini's two-dimensional model. Hysteresis loss measurements in a series of fine-filament Nb_3Sn superconductors showed that the effective filament diameter is a function of interfilament separation and local area ratio of matrix material to Nb. A review of internal fields in superconductors showed the importance of demagnetization factors and internal fields for the correct analysis of magnetic data. A theoretical method of calibrating ac susceptometers for cylindrical specimens, which is based on a mutual-inductance calculation, was developed.

12. KEY WORDS (Six to twelve entries; alphabetical order; capitalize only proper names; and separate key words by semicolons)

ac losses; hysteresis; magnetization; magnetometers; niobium-tin; niobium-titanium; superconductors; susceptibility; susceptometers; transient losses.

13. AVAILABILITY

☒ Unlimited
☐ For Official Distribution. Do Not Release to NTIS
☐ Order From Superintendent of Documents, U.S. Government Printing Office, Washington, D.C. 20402.
☐ Order From National Technical Information Service (NTIS), Springfield, VA. 22161

14. NO. OF PRINTED PAGES
72

15. Price

USCOMM-DC 6043-P80

☆ U. S. GOVERNMENT PRINTING OFFICE: 1986—672-376/45,268 REGION NO. 8

END

12-86

DTIC